

Towards Flexibility and Interpretability of Gaussian Process State-Space Model

Zhidi Lin, Feng Yin, *Senior Member, IEEE*

Abstract—Gaussian process state-space model (GPSSM) has attracted much attention over the past decade. However, the model representation power of GPSSM is far from satisfactory. Most GPSSM works rely on the standard Gaussian process (GP) with a preliminary kernel, such as squared exponential (SE) kernel and Matérn kernel, which limit the model representation power and its application in complex scenarios. To address this issue, this paper proposes a novel class of probabilistic state-space model named TGPSSM that enriches the GP priors in the standard GPSSM through parametric normalizing flow, making the state-space model more flexible and expressive. In addition, by inheriting the advantages of sparse representation of GP models, we propose a scalable and interpretable variational learning algorithm to learn the TGPSSM and infer the latent dynamics simultaneously. By integrating a constrained optimization framework and explicitly constructing a non-Gaussian state variational distribution, the proposed learning algorithm enables the TGPSSM to significantly improve the capabilities of state space representation and model inference. Experimental results based on various synthetic and real datasets corroborate that the proposed TGPSSM yields superior learning and inference performance compared to several state-of-the-art methods. The accompanying source code is available at <https://github.com/zhidilin/TGPSSM>.

Index Terms—Gaussian process, state-space model, normalizing flow, variational learning and inference.

I. INTRODUCTION

BECAUSE of the superiority in modeling dynamical systems, state-space models (SSMs) have been successfully applied in various fields of engineering, statistics, computer science, and economics [1]. A generic SSM describes the underlying system dynamics and the dependence between the latent states $\mathbf{x}_t \in \mathbb{R}^{d_x}$ and the observations $\mathbf{y}_t \in \mathbb{R}^{d_y}$. Mathematically, it can be written as

$$\mathbf{x}_{t+1} = f(\mathbf{x}_t) + \mathbf{v}_t, \quad (1a)$$

$$\mathbf{y}_t = g(\mathbf{x}_t) + \mathbf{e}_t, \quad (1b)$$

where $f(\cdot) : \mathbb{R}^{d_x} \mapsto \mathbb{R}^{d_x}$ and $g(\cdot) : \mathbb{R}^{d_x} \mapsto \mathbb{R}^{d_y}$ are transition function and emission function, respectively; \mathbf{v}_t and \mathbf{e}_t are additive noise terms. The two major tasks with SSMs are learning and inference. Learning in SSM, also known as system identification, is about finding optimal model parameters so that the underlying dynamical system can be accurately captured, while inference in SSM refers to optimally estimating the latent states of interest using the observed sequential data [1].

A plethora of learning and inference methods for SSM have been developed in the past decades. For example, when the

system dynamics are exactly known, the Kalman filter (KF), extended Kalman filter (EKF), unscented Kalman filter (UKF), and particle filter (PF) can be used to estimate the latent states [1]. However, for some complex and harsh scenarios, such as model based reinforcement learning [2], and disease epidemic propagation [3], the underlying system dynamics are hard to be well determined *a priori* [4]. Thus, the dynamics need to be learned from the observed noisy measurements, leading to the emergence of data-driven state-space models. The representative classes of the data-driven state-space models include the deep state-space models (DSSMs) [3]–[7] and the Gaussian process state-space models (GPSSMs) [8]–[19], which employ deep neural networks [20] or Gaussian processes (GPs) [21] as the core data-driven module to model the underlying unknown and possibly complex system dynamics.

Because of the powerful model representation capability of deep neural networks, the DSSMs are able to model complex and high-dimensional dynamical systems, and have shown impressive results in some real-world applications, such as disease progression analysis [3], medications effect analysis [6], and nonlinear system identification [7]. However, several vital limitations exist in DSSMs: 1) The transition and/or emission functions in DSSMs are modeled by deep neural networks that typically require a huge amount of data to tune the large number of model parameters. In other words, DSSMs are not data-efficient; 2) DSSMs using deep neural networks are black-box models without interpretability, which is risky to use for (safety)-critical applications [22]; 3) Because of the deterministic deep neural networks, there is no explicit uncertainty quantification for the transition/emission functions in DSSMs as well as their predictions [15].

In contrast, the class of GPSSMs is able to naturally address the above-mentioned limitations. First, GPSSM is a popular class of probabilistic SSM that is well interpretable and naturally counts for model uncertainty in a fully Bayesian way [12]. Second, the nonparametric GP model adopted in the GPSSM, known as a data-efficient model, is directly parameterized by data and can automatically adapt the model complexity to the observations [20], thus it is suitable for learning from small datasets [21].

Due to the appealing properties of the GPSSMs, much promising progress has been made over the past decade. Early GPSSM works proposed various learning and inference methods [8], [9], [23], [24] for the applications of robotics control [25], human motion modeling [26], and so on. However, these methods either estimate the latent states by performing a *maximum a posteriori*, or learn the transition function by assuming the observable latent states, resulting in limited use

Zhidi Lin and Feng Yin are with the School of Science and Engineering, The Chinese University of Hong Kong, Shenzhen 518172, China (e-mail: zhidilin@link.cuhk.edu.cn, yinfeng@cuhk.edu.cn). *Feng Yin is the corresponding author.*

cases of the GPSSM. The first Bayesian treatment of learning and inference in GPSSM was proposed in [10] using Monte Carlo sampling methods, which entails high computational complexity and is prohibitive to high-dimensional latent states. To this end, attention was shifted later to variational approximation based methods [11]–[19], which can be divided into two classes: the mean-field (MF) one [11]–[14] and the non-mean-field (NMF) one [15]–[19], according to whether the independence assumption between the GP-modeled transition function and the latent states is made in designing a variational distribution. More specifically, the first MF variational algorithm that integrates the particle filter was proposed in [11]. Authors in [14] assumed a linear Markov Gaussian variational distribution for the latent states and additionally employed an inference network to overcome the issue of linear growth of the number of variational parameters over time. The first NMF variational algorithm was proposed in [15], where the posterior of latent states is directly approximated using the prior distribution. Later on, different nonlinear and parametric Markov Gaussian distributions were employed to approximate the posterior of the latent states, hence leading to different NMF algorithms [16]–[19]. These variational algorithms have their advantages and disadvantages, but in general, the MF class is simpler and less computationally expensive than the NMF class. In [27], [28], online GPSSM learning schemes were proposed. However, the emission function in the GPSSM was modeled using deep Gaussian process [28], which can cause severe non-identifiability issue, see discussions in Section II-B. Other recent works lie in applying GPSSM to different applications by fusing the knowledge of physical models when learning the GPSSM [29]–[31].

Even though the learning and inference algorithm is one of the key elements of GPSSM, the model representation power still limits its learning and inference performance, which has been neglected over the past years. Compared to DSSM, the current works on GPSSM are still incapable for modeling complex nonlinear dynamical systems due to its limited representation power using elementary GP kernels. Therefore, it is imperative to increase the model capacity of GPSSM to meet the requirements of modeling complex dynamical systems. There are two different paths to boost the model representation power: 1) Transforming the standard GP equipped with elementary kernel into a more flexible stochastic process to be the new function prior [32]–[34]; 2) Applying universal/optimal kernels in the GP model [35]–[39]. We note that although path 2) can improve the flexibility of the GP by adopting an optimal kernel function, the Gaussianity in the GP may be still limited and inappropriate for modeling complex systems [32]. In addition, using optimal kernels, e.g., spectral mixture kernels [35]–[37] or deep kernels [38], [39], usually involves a large number of kernel hyperparameters. Therefore, the model training/optimization process will be more computationally expensive and sensitive to the initialization [36]. Thus, this paper focuses on the first path to transform the standard GP prior to a more flexible stochastic process that maintains the elegance and interpretability of GP while requiring fewer model hyperparameters to be tuned. More specifically, we exploit the normalizing flow technique [40]

to improve the model representation power of the GPSSM, thereby improving the learning and inference performance in harsh and extreme scenarios. The main contributions of this paper are detailed as follows:

- We propose a flexible and expressive class of probabilistic SSMs, called transformed Gaussian process state-space models (TGPSSMs), by leveraging the normalizing flow technique [40], [41] to transform the GP priors in GPSSM. Theoretically, the proposed TGPSSM can be regarded as putting a flexible stochastic process prior over the classic state-space models, which provides a unified framework for standard probabilistic state-space models, including GPSSM.
- To learn the TGPSSM and simultaneously infer the latent dynamics without high computational costs, we leverage the advantages inherited from the sparse GP [42] and propose an interpretable and scalable variational learning and inference algorithm.
- Instead of assuming a joint Gaussian variational distribution, we explicitly construct a more flexible one that could be non-Gaussian for the proposed variational learning algorithm, and integrate a constrained optimization framework to improve the inference and state-space representation capabilities.
- Extensive numerical tests based on various synthesized and real-world datasets verify that the proposed flexible TGPSSM empowered by the variational learning algorithm provides improved model learning and inference performance compared with several competing methods.

The remainder of this paper is organized as follows. Some preliminaries related to GPSSMs are provided in Section II. Section III details the proposed flexible and expressive TGPSSM. Section IV elaborates the proposed variational learning and inference algorithms. Experimental results are given in Section V, and finally Section VI concludes this paper. Some supportive results, proofs, and detailed derivations are given in the supplementary Appendix available online.

II. PRELIMINARIES

This section provides some preliminaries for GPSSM. Concretely, Section II-A briefly reviews the Gaussian process for machine learning, especially the regression task, and Section II-B briefly introduces the GPSSM and its fundamental properties.

A. Gaussian Process (GP)

GP defines a collection of random variables indexed by $\mathcal{X} \subseteq \mathbb{R}^{d_x}$, such that any finite collection of these variables follows a joint Gaussian distribution [21]. Mathematically, a real scalar-valued Gaussian process $f(\mathbf{x})$ can be written as

$$f(\mathbf{x}) \sim \mathcal{GP}(\mu(\mathbf{x}), k(\mathbf{x}, \mathbf{x}'); \boldsymbol{\theta}_{gp}) \quad (2)$$

where $\mu(\mathbf{x})$ is a mean function and is typically set to zero in practice; $k(\mathbf{x}, \mathbf{x}')$ is the covariance function, a.k.a. kernel function, and $\boldsymbol{\theta}_{gp}$ is a set of hyperparameters that needs to be

tuned for model selection. Considering a general regression model,

$$y = f(\mathbf{x}) + e, \quad e \sim \mathcal{N}(0, \sigma_e^2), \quad y \in \mathbb{R}, \quad (3)$$

we wish to learn the mapping function $f(\cdot) : \mathbb{R}^{d_x} \mapsto \mathbb{R}$ using an observed dataset $\mathcal{D} \triangleq \{\mathbf{x}_i, y_i\}_{i=1}^n \triangleq \{\mathbf{X}, \mathbf{y}\}$ consisting of n samples, or alternatively input-output pairs. By placing a GP prior over the function $f(\cdot)$ in Eq. (3), we get the salient Gaussian process regression (GPR) model. Conditioning on the observed data, the posterior distribution of the mapping function, $p(f(\mathbf{x}_*) | \mathbf{x}_*, \mathcal{D})$, at any test input $\mathbf{x}_* \in \mathcal{X}$ is Gaussian, fully characterized by the posterior mean ξ and the posterior variance Ξ . Concretely,

$$\xi(\mathbf{x}_*) = \mathbf{K}_{\mathbf{x}_*, X} (\mathbf{K}_{X, X} + \sigma_e^2 \mathbf{I}_n)^{-1} \mathbf{y}, \quad (4a)$$

$$\Xi(\mathbf{x}_*) = k(\mathbf{x}_*, \mathbf{x}_*) - \mathbf{K}_{\mathbf{x}_*, X} (\mathbf{K}_{X, X} + \sigma_e^2 \mathbf{I}_n)^{-1} \mathbf{K}_{\mathbf{x}_*, X}^\top, \quad (4b)$$

where $\mathbf{K}_{X, X}$ denotes the covariance matrix evaluated on the training input X , and each entry is $[\mathbf{K}_{X, X}]_{i, j} = k(\mathbf{x}_i, \mathbf{x}_j)$; $\mathbf{K}_{\mathbf{x}_*, X}$ denotes the cross covariance matrix between the test input \mathbf{x}_* and the training input X ; The zero-mean GP prior is assumed here and will be used in the rest of this paper if there is no other specification. Note that the posterior distribution $p(f(\mathbf{x}_*) | \mathbf{x}_*, \mathcal{D})$ gives not only a point estimate, i.e., the posterior mean, but also the uncertainty region of such estimate quantified by the posterior variance.

B. Gaussian Process State-Space Model (GPSSM)

Placing GP priors over both transition function $f(\cdot)$ and emission function $g(\cdot)$ in SSM (c.f. Eq. (1)) leads to the well-known Gaussian process state-space model (GPSSM). However, such GPSSM with transition and emission GPs incurs severe non-identifiability issue between $f(\cdot)$ and $g(\cdot)$ [11]. To address this issue, GPSSM with GP transition and parametric emission is considered in literature, as it keeps the same model capacity as the original GPSSM with transition and emission GPs, though it requires to introduce a higher dimensional augmented latent states [12]. The result is summarized by the following theorem.

Theorem 1. For the GPSSM with both transition and emission GPs,

$$\mathbf{x}_{t+1} = f(\mathbf{x}_t) + \mathbf{v}_t, \quad f(\cdot) \sim \mathcal{GP}, \quad (5a)$$

$$\mathbf{y}_t = g(\mathbf{x}_t) + \mathbf{e}_t, \quad g(\cdot) \sim \mathcal{GP}, \quad (5b)$$

by defining the augmented state $\bar{\mathbf{x}}_{t+1} = [\mathbf{x}_{t+1}, \gamma_t]^\top$, Gaussian process $h(\bar{\mathbf{x}}_t) = [f(\mathbf{x}_t), g(\mathbf{x}_t)]^\top$, and the augmented process noise $\mathbf{w}_t = [\mathbf{v}_t, \mathbf{0}]^\top$, the original model in Eq. (5) can be reformulated to a GPSSM with GP transition and a simple parametric emission,

$$\bar{\mathbf{x}}_{t+1} = h(\bar{\mathbf{x}}_t) + \mathbf{w}_t, \quad h(\cdot) \sim \mathcal{GP}, \quad (6a)$$

$$\mathbf{y}_t = \gamma_t + \mathbf{e}_t, \quad (6b)$$

so as to eliminate/alleviate the severe non-identifiability issue.

The interested reader can refer to [12] (Section 3.2.1) for more details. Thus, in keeping with previous literature and without loss of generality, we mainly consider the GPSSM

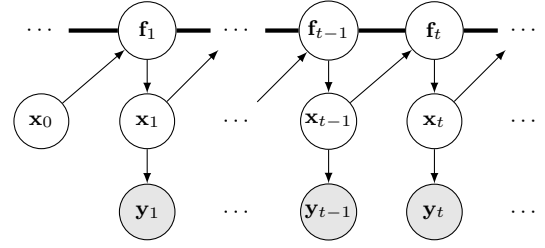


Fig. 1: Graphical model of a GPSSM with GP transition and parametric emission. The circles with gray color and white color mean the variables are observable and latent, respectively. The thick horizontal bar represents a set of fully connected nodes, i.e., the Gaussian process.

depicted in Fig. 1 in the rest of this paper, where a GP prior is placed over the state transition function $f(\cdot)$. The model is expressed by the following equations:

$$f(\cdot) \sim \mathcal{GP}(\mu(\cdot), k(\cdot, \cdot); \boldsymbol{\theta}_{gp}) \quad (7a)$$

$$\mathbf{x}_0 \sim p(\mathbf{x}_0) \quad (7b)$$

$$\mathbf{f}_t = f(\mathbf{x}_{t-1}) \quad (7c)$$

$$\mathbf{x}_t | \mathbf{f}_t \sim \mathcal{N}(\mathbf{x}_t | \mathbf{f}_t, \mathbf{Q}) \quad (7d)$$

$$\mathbf{y}_t | \mathbf{x}_t \sim \mathcal{N}(\mathbf{y}_t | \mathbf{C}\mathbf{x}_t, \mathbf{R}) \quad (7e)$$

where the latent states form a Markov chain, that is, for any time instance t , the future state \mathbf{x}_{t+1} is generated by conditioning on only \mathbf{x}_t and the GP transition $f(\cdot)$. According to Theorem 1, the parametric emission model is assumed to be known and restricted to be a linear mapping with the coefficient matrix $\mathbf{C} \in \mathbb{R}^{d_y \times d_x}$. Both the state transitions and observations are corrupted by zero-mean Gaussian noise with covariance matrices \mathbf{Q} and \mathbf{R} , respectively.

If the state is multidimensional, i.e. $d_x > 1$, the system transition/dynamics, $f(\cdot) : \mathbb{R}^{d_x} \mapsto \mathbb{R}^{d_x}$, is typically modeled by using d_x mutually independent GPs. More concretely, each output dimension-specific function, $f_d(\cdot) : \mathbb{R}^{d_x} \mapsto \mathbb{R}$, is independently modeled by a scalar-valued GP, and we denote:

$$\mathbf{f}_t = f(\mathbf{x}_{t-1}) \triangleq \{f_d(\mathbf{x}_{t-1})\}_{d=1}^{d_x}, \quad (8)$$

where each independent GP has its own mean and kernel functions $\mu_d(\cdot)$ and $k_d(\cdot, \cdot)$. Finally, note that GPSSM depicted in Fig. 1 can be easily extended to a control system with deterministic control input $\mathbf{c}_t \in \mathbb{R}^{d_c}$ through an augmented latent state $\bar{\mathbf{x}}_t = [\mathbf{x}_t, \mathbf{c}_t] \in \mathbb{R}^{d_x + d_c}$, but for notation brevity, we omit \mathbf{c}_t throughout this paper.

To ease our notation in the rest of discussions, we introduce the following short-hand notations. Let an observation sequence of length T be $\mathbf{Y} \triangleq \mathbf{y}_{1:T} = \{\mathbf{y}_1, \mathbf{y}_2, \dots, \mathbf{y}_T\}$, latent function variables $\mathbf{F} \triangleq \mathbf{f}_{1:T} = \{\mathbf{f}_1, \mathbf{f}_2, \dots, \mathbf{f}_T\}$, and latent states $\mathbf{X} \triangleq \mathbf{x}_{0:T} = \{\mathbf{x}_0, \mathbf{x}_1, \dots, \mathbf{x}_T\}$. Based on the aforementioned model settings, the joint density function of the GPSSM depicted in Fig. 1 can be written as:

$$p(\mathbf{F}, \mathbf{X}, \mathbf{Y} | \boldsymbol{\theta}) = p(\mathbf{x}_0) p(\mathbf{f}_{1:T}) \prod_{t=1}^T p(\mathbf{y}_t | \mathbf{x}_t) p(\mathbf{x}_t | \mathbf{f}_t) \quad (9)$$

where $p(\mathbf{f}_{1:T}) = p(f(\mathbf{x}_{0:T-1}))$ corresponds to the finite-dimensional GP distribution. The model parameters $\boldsymbol{\theta}$ includes the noise and GP hyper-parameters, i.e., $\boldsymbol{\theta} = [\mathbf{Q}, \mathbf{R}, \boldsymbol{\theta}_{gp}]$. The

challenging task in GPSSM is to learn the θ , and simultaneously infer the latent states of interest from a set of observation $\mathbf{y}_{1:T}$.

III. PROPOSED MODEL

As mentioned in Section I, the model representation power of GPSSM using elementary kernels is still limited. This section aims to address the model representation power issue, thereby improving the learning and inference performance of GPSSM. By exploiting the parametric normalizing flow technique [40], we propose a flexible and interpretable probabilistic SSM, and we detail each of its components in this section. Specifically, leveraging the parametric normalizing flow, we introduce a more flexible function prior, namely the transformed Gaussian process (TGP) in Section III-A. Different normalizing flows for TGP construction under practical usage considerations are detailed in Section III-B. Lastly, we introduce our proposed probabilistic SSM in Section III-C.

A. Transformed Gaussian Process (TGP)

Normalizing flow was originally proposed to transform a simple random variable into a more complex one by applying a sequence of invertible and differentiable transformations (i.e., the *diffeomorphisms*) [40]. Specifically, let \mathbf{x} be a d_x -dimensional continuous random vector, and $p(\mathbf{x})$ be the corresponding probability density distribution. Normalizing flow can help construct a desired, often more complex and possibly multi-modal distribution by pushing \mathbf{x} through a series of transformations, $\mathbb{G}_{\theta_F}(\cdot) = \mathbb{G}_{\theta_0} \circ \mathbb{G}_{\theta_1} \circ \dots \circ \mathbb{G}_{\theta_{J-1}}$, i.e.,

$$\tilde{\mathbf{x}} = \mathbb{G}_{\theta_{J-1}}(\mathbb{G}_{\theta_{J-2}}(\dots \mathbb{G}_{\theta_0}(\mathbf{x})\dots)), \quad (10)$$

where the set of J transformations, $\{\mathbb{G}_{\theta_j}(\cdot) : \mathbb{R}^{d_x} \mapsto \mathbb{R}^{d_x}\}_j^{J-1}$ parameterized by $\theta_F \triangleq [\theta_0, \theta_1, \dots, \theta_{J-1}]$, have to be invertible and differentiable [41]. Under these conditions, the probability density of the induced random vector, $\pi(\tilde{\mathbf{x}})$, is well-defined and can be obtained by the ‘‘change of variables’’ formula, yielding:

$$\pi(\tilde{\mathbf{x}}) = p(\mathbf{x}) \underbrace{\prod_{j=0}^{J-1} \left| \det \frac{\partial \mathbb{G}_{\theta_j}(\mathbb{G}_{\theta_{j-1}}(\dots \mathbb{G}_{\theta_0}(\mathbf{x})\dots))}{\partial \mathbb{G}_{\theta_{j-1}}(\dots \mathbb{G}_{\theta_0}(\mathbf{x})\dots)} \right|^{-1}}_{\triangleq \mathbf{J}_{\mathbf{x}}}. \quad (11)$$

We refer readers to [40], [41] for more details.

Motivated by the normalizing flow applied to random variables, for the complex system dynamics that the standard GP equipped with elementary kernels cannot model, a good way is to transform the GP prior. Applying the same idea as the normalizing flow on random variables, we can transform the standard GP $f(\cdot)$ into a more flexible and expressive random process $\tilde{f}(\cdot)$. Specifically, we define the transformed Gaussian process (TGP) as follows.

Definition 1 (Transformed Gaussian process). *A transformed Gaussian process, $\tilde{f}(\cdot)$, is a collection of random variables, such that any finite collection, $\{\tilde{f}(\mathbf{x}_1), \tilde{f}(\mathbf{x}_2), \dots, \tilde{f}(\mathbf{x}_T)\}$, $T \in \mathbb{N}$, has joint distribution defined by the following generative equations:*

$$\tilde{\mathbf{f}}_t = \tilde{f}(\mathbf{x}_t) = \mathbb{G}_{\theta_F}(\mathbf{f}_t), \quad \mathbf{f}_t = f(\mathbf{x}_t), \quad \forall t = 1, 2, \dots, T, \quad (12)$$

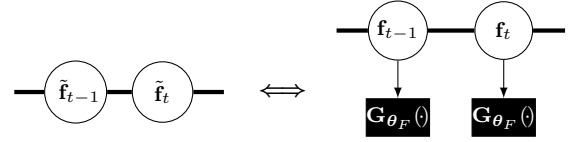


Fig. 2: Equivalent representations of TGP prior, $\tilde{\mathbf{f}}_t, \forall t$. The black square blocks represent parametric transformation and the circles represent random variables. The thick horizontal bar represents a set of fully connected nodes, i.e., instances of a stochastic process.

where $\mathbb{G}_{\theta_F}(\cdot) : \mathbb{R}^{d_x} \mapsto \mathbb{R}^{d_x}$ is a invertible and differentiable mapping parameterized by the parameters θ_F , and \mathbf{f}_t is a Gaussian random variable from the standard Gaussian process, $f(\cdot)$, indexed by any input $\mathbf{x}_t \in \mathcal{X}$.

Figure 2 shows two equivalent graphical representations of the TGP prior. The mapping $\mathbb{G}_{\theta_F}(\cdot)$ defined in Eq. (12) that transforms the standard GP coordinate-wisely is called the marginal flow or marginal transport in the literature [33], [34]. It has been formally proved in [33] that a scalar-valued stochastic process transformed by marginal flow induces a valid stochastic process. The result can be extended to vector-valued GP [43], which is summarized in the following corollary.

Corollary 1. *Given a marginal flow, $\mathbb{G}_{\theta_F}(\cdot)$, and a multidimensional Gaussian process $f(\cdot)$ [43] with input space \mathcal{X} , the transformed process denoted as $\tilde{f} \triangleq \mathbb{G}_{\theta_F}(f)$, is a valid multivariate stochastic process in the same input space.*

Proof. First, since $\mathbb{G}_{\theta_F}(\cdot)$ is invertible and differentiable, the push-forward measure is well-defined. Then, any collection of finite-dimensional distributions $\{\tilde{\mathbf{f}}_1, \tilde{\mathbf{f}}_2, \dots, \tilde{\mathbf{f}}_T\}$, $T \in \mathbb{N}$ from \tilde{f} , satisfy the consistency conditions of the well-known *Kolmogorov’s consistency theorem* [44], due to the marginal flows being coordinate-wise maps, which complete the proof. \square

According to the TGP definition, the probability distribution of any finite collection of TGP, $\tilde{\mathbf{f}}_{1:T} = \{\tilde{\mathbf{f}}_1, \tilde{\mathbf{f}}_2, \dots, \tilde{\mathbf{f}}_T\}$, is

$$p(\tilde{\mathbf{f}}_{1:T}) = p(\tilde{f}(\mathbf{x}_{1:T})) = p(\mathbf{f}_{1:T}) \mathbf{J}_{\mathbf{f}} \quad (13)$$

where $\mathbf{J}_{\mathbf{f}} \triangleq \prod_{j=0}^{J-1} \left| \det \frac{\partial \mathbb{G}_{\theta_j}(\mathbb{G}_{\theta_{j-1}}(\dots \mathbb{G}_{\theta_0}(\mathbf{f}_{1:T})\dots))}{\partial \mathbb{G}_{\theta_{j-1}}(\dots \mathbb{G}_{\theta_0}(\mathbf{f}_{1:T})\dots)} \right|^{-1}$. With the marginal flow $\mathbb{G}_{\theta_F}(\cdot)$, any finite-dimensional distribution of TGP $p(\tilde{f}(\mathbf{x}_{1:T}))$ can be non-Gaussian, thus the obtained TGP is a more flexible and expressive function prior. It is noteworthy that using the idea of transformation to improve the representation power was proposed as early as the 1960s, such as the most representative Box-Cox transformation for the standard linear regression models [45]. The transformed GP priors leveraging parametric transformation is in line with several existing works, such as transport GP [33], [34] and warped GP [46], [47]. However, these works mainly focus on scalar-valued supervised learning tasks instead of learning and inference in SSMs with multidimensional latent state space. If the transformation is constructed by the multi-layered GPs, then this leads to the deep Gaussian process (DGP) model [32]. However, training the DGP is essentially challenging because of the high computational complexity involved during the training phase [33], [34], [48]. In this paper, we concentrate on leveraging normalizing flows to increase the

model representation power in the original GPSSM without substantially increasing the overall computational complexity.

B. Construction and Usage of Normalizing Flow

This subsection introduces the practical guidelines for constructing and using normalizing flows. In principle, any normalizing flows can be applied to the TGP model, such as the simpler but interpretable elementary flows and the more advanced data-driven ones proposed in recent years [40], [41]. However, when some prior knowledge about underlying system dynamics is available, we tend to use the elementary flows because of their superior interpretability and fewer model parameters compared to the data-driven ones. Table I presents several well-studied and interpretable elementary flows, along with their possible flow compositions used in literature. For example, if the latent states in SSMs are known to have a large dispersion, then the latent states follow a heavy-tailed distribution. In this case, the Sinh-Arcsinh transformations can be used to control the mean, variance, asymmetry, and kurtosis [50] of the TGP prior when modeling the system dynamics. Another example is that one can compose two affine-logarithmic transformations to handle the bounded data [33].

However, the elementary flows and their compositions may be still insufficient, especially when modeling the dynamical system in extremely harsh and complex scenarios. To this end, the normalizing flows developed recently can be integrated with GP prior to increase the model flexibility, such as the real-valued non-volume preserving (RealNVP) flow [51] and continual normalizing flow [52]. In this paper, we utilize the RealNVP flow as an example to model multidimensional TGP because of its universal approximation capability and competitive performance compared to other competitors in terms of the number of model parameters and the training speed [53]. The transformations $\mathbb{G}_{\theta_j}(\cdot)$, $j = 0, 1, \dots, J-1$, in RealNVP are constructed by coupling layers. Specifically, given a d_x -dimensional function output, $\mathbf{f}_t = [\mathbf{f}_{t,1}, \mathbf{f}_{t,2}, \dots, \mathbf{f}_{t,d_x}]^\top \in \mathbb{R}^{d_x}$, and $d < d_x$, the first coupling layer output, $\mathbf{f}_t^{(1)} = [\mathbf{f}_{t,1}^{(1)}, \mathbf{f}_{t,2}^{(1)}, \dots, \mathbf{f}_{t,d_x}^{(1)}]^\top$, follows the equations

$$\mathbf{f}_{t,1:d}^{(1)} = \mathbf{f}_{t,1:d}, \quad (14a)$$

$$\mathbf{f}_{t,d+1:d_x}^{(1)} = \mathbf{f}_{t,d+1:d_x} \odot \exp(s_1(\mathbf{f}_{t,1:d})) + r_1(\mathbf{f}_{t,1:d}), \quad (14b)$$

where $s_1(\cdot)$ and $r_1(\cdot)$ are arbitrary complex mappings $\mathbb{R}^d \mapsto \mathbb{R}^{d_x-d}$, which can be modeled by neural networks, and \odot represents element-wise product. Then by stacking coupling layers in an alternating fashion, elements that are unchanged in the last coupling layer are updated in the next [51]. Note that if the elements of the function output, $\{\mathbf{f}_{t,1}, \mathbf{f}_{t,2}, \dots, \mathbf{f}_{t,d_x}\}$, are independent, the outputs of the RealNVP flow, e.g., $\{\mathbf{f}_{t,1}^{(1)}, \mathbf{f}_{t,2}^{(1)}, \dots, \mathbf{f}_{t,d_x}^{(1)}\}$, are dependent because of the transformation of the J coupling layers.

C. Transformed Gaussian Process State-Space Model

Placing a TGP prior $\tilde{f}(\cdot)$ defined in Section III-A over the transition function of SSM gives rise to the transformed Gaussian process state-space model (TGPSSM). The corresponding

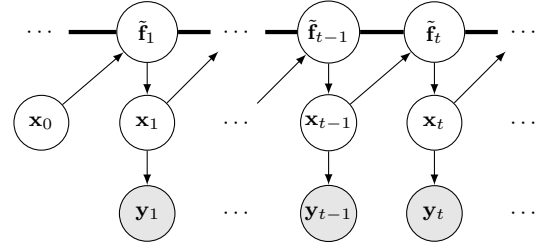


Fig. 3: Graphical model of TGPSSM. The circles with gray color and white color mean the variables are observable and latent, respectively. The thick horizontal bar represents a set of fully connected nodes, i.e., the transformed Gaussian process.

graphical model is shown in Fig. 3. Mathematically, the model can be expressed by the following set of equations:

$$\tilde{f}(\cdot) = \mathbb{G}_{\theta_F}(f), \quad f(\cdot) \sim \mathcal{GP}(\mu(\cdot), k(\cdot, \cdot); \theta_{gp}) \quad (15a)$$

$$\mathbf{x}_0 \sim p(\mathbf{x}_0) \quad (15b)$$

$$\mathbf{f}_t = f(\mathbf{x}_{t-1}) \quad (15c)$$

$$\tilde{\mathbf{f}}_t = \mathbb{G}_{\theta_F}(\mathbf{f}_t) = \tilde{f}(\mathbf{x}_{t-1}) \quad (15d)$$

$$\mathbf{x}_t | \tilde{\mathbf{f}}_t \sim \mathcal{N}(\mathbf{x}_t | \tilde{\mathbf{f}}_t, \mathbf{Q}) \quad (15e)$$

$$\mathbf{y}_t | \mathbf{x}_t \sim \mathcal{N}(\mathbf{y}_t | \mathbf{C}\mathbf{x}_t, \mathbf{R}) \quad (15f)$$

where $\mathbb{G}_{\theta_F}(\cdot)$ is a marginal flow described in Section III-A. For a sequence of size T , we denote the corresponding TGP function values as $\tilde{\mathbf{F}} \triangleq \tilde{\mathbf{f}}_{1:T}$. The joint probability density function of the above TGPSSM is

$$p(\tilde{\mathbf{F}}, \mathbf{X}, \mathbf{Y} | \theta) = p(\mathbf{x}_0) p(\tilde{\mathbf{f}}_{1:T}) \prod_{t=1}^T p(\mathbf{x}_t | \tilde{\mathbf{f}}_t) p(\mathbf{y}_t | \mathbf{x}_t), \quad (16)$$

where $p(\tilde{\mathbf{f}}_{1:T}) = p(\tilde{f}(\mathbf{x}_{0:T-1}))$ corresponds to the finite-dimensional TGP distribution, and the model parameters $\theta = [\theta_{gp}, \theta_F, \mathbf{Q}, \mathbf{R}]$. Sampling from the TGPSSM prior is similar to sampling from GPSSM prior [12], except requiring an extra transformation step that transforms the sampled latent function value \mathbf{f}_t to get $\tilde{\mathbf{f}}_t$. Detailed sampling steps and examples can be found in Appx. A.

Remark 1 (Dependency constructions). *In the original GPSSM, the d_x -dimensional ($d_x > 1$) system dynamics are modeled by d_x mutually independent GP priors, which is simplifying but may be unrealistic. In contrast, the corresponding d_x -dimensional TGP prior is generally not independent due to normalizing flows (e.g., the RealNVP). Therefore, placing TGP prior over SSMs not only enables more flexible system dynamics modeling, but also establishes the dependencies between dimensions of latent state in SSMs, which can be beneficial for state inference [19].*

Generally, the computational complexity of TGPSSM mainly comes from the computation of standard GP model. For instance, sampling from TGPSSM as shown in Appx. A, scales as $\mathcal{O}(d_x T^3)$, which is prohibitive for big data. To address the computational issue, we leverage the sparse GP [42] to alleviate the high computational complexity in the TGPSSM. By introducing sparse GP to augment the GP prior with M inducing points $\mathbf{U} \triangleq \mathbf{u}_{1:M} = \{\mathbf{u}_1, \mathbf{u}_2, \dots, \mathbf{u}_M\}$ at locations

TABLE I: Elementary flows and their compositional flows

Elementary Flow	Arcsinh	Log	Exp	Linear	Sinh-Arcsinh	Box-Cox	Tanh
	$a + b \operatorname{arcsinh}[d(\mathbf{f} - c)]$, $a, b, c, d \in \mathbb{R}$	$\log(\mathbf{f})$	$\exp(\mathbf{f})$	$a + b\mathbf{f}$, $a, b \in \mathbb{R}$	$\sinh[b \operatorname{arcsinh}(\mathbf{f}) - a]$, $a, b \in \mathbb{R}$	$\frac{1}{\lambda} \left(\operatorname{sgn}(\mathbf{f}) \mathbf{f} ^\lambda - 1 \right)$, $\lambda > 0$	$a \tanh[b(\mathbf{f} + c)] + d$, $a, b, c, d \in \mathbb{R}$
Flow Composition	Sum of Log-Exp [49]			Sinh-Arcsinh-Linear (SAL) [33]		Sum of Tanh [46]	
	$\sum_{j=0}^{J-1} a_j \log(1 + \exp[b_j(\mathbf{f} + c_j)])$, $a_j, b_j \geq 0, \forall j$			$d \sinh(b \operatorname{arcsinh}(\mathbf{f}) - a) + c$, $a, b, c, d \in \mathbb{R}$		$\mathbf{f} + \sum_{j=0}^{J-1} a_j \tanh[b_j(\mathbf{f} + c_j)]$, $a_j, b_j \geq 0, \forall j$	

• If the input argument \mathbf{f} is multidimensional, the flows transform \mathbf{f} element-wisely.

$\mathbf{Z} \triangleq \mathbf{z}_{1:M} = \{\mathbf{z}_1, \mathbf{z}_2, \dots, \mathbf{z}_M\}$, i.e., $\mathbf{u}_{1:M} = f(\mathbf{z}_{1:M})$, the TGP prior after introducing the sparse inducing points is given by

$$p(\tilde{\mathbf{F}}, \tilde{\mathbf{U}}) = p(\tilde{\mathbf{f}}_{1:T}, \tilde{\mathbf{u}}_{1:M}) = \underbrace{p(\mathbf{F}|\mathbf{U})\mathbf{J}_{\mathbf{f}}}_{=p(\tilde{\mathbf{F}}|\tilde{\mathbf{U}})} \cdot \underbrace{p(\mathbf{U})\mathbf{J}_{\mathbf{u}}}_{=p(\tilde{\mathbf{U}})}, \quad (17)$$

where $p(\mathbf{U})$ is the sparse GP distribution, $p(\mathbf{F}|\mathbf{U})$ is the corresponding noiseless GP posterior defined in Eq. (4), $\tilde{\mathbf{U}} \triangleq \tilde{\mathbf{u}}_{1:M} = \tilde{f}(\mathbf{z}_{1:M})$, and

$$\mathbf{J}_{\mathbf{f}} = \prod_{j=0}^{J-1} \left| \det \frac{\partial \mathbb{G}_{\theta_j}(\mathbb{G}_{\theta_{j-1}}(\dots \mathbb{G}_{\theta_0}(\mathbf{F})\dots))}{\partial \mathbb{G}_{\theta_{j-1}}(\dots \mathbb{G}_{\theta_0}(\mathbf{F})\dots)} \right|^{-1}, \quad (18a)$$

$$\mathbf{J}_{\mathbf{u}} = \prod_{j=0}^{J-1} \left| \det \frac{\partial \mathbb{G}_{\theta_j}(\mathbb{G}_{\theta_{j-1}}(\dots \mathbb{G}_{\theta_0}(\mathbf{U})\dots))}{\partial \mathbb{G}_{\theta_{j-1}}(\dots \mathbb{G}_{\theta_0}(\mathbf{U})\dots)} \right|^{-1}. \quad (18b)$$

Detailed derivations of Eq. (17) can be found in Appx. B, where we use the fact that the coordinate-wise mapping $\mathbb{G}_{\theta_F}(\cdot)$, induces a valid TGP and in turn, guarantee that the transformed sparse GP is consistent [33]. Therefore, the joint distribution of the TGPSSM augmented by inducing points is

$$p(\tilde{\mathbf{F}}, \tilde{\mathbf{U}}, \mathbf{X}, \mathbf{Y}) = p(\mathbf{x}_0) p(\tilde{\mathbf{f}}_{1:T}, \tilde{\mathbf{u}}_{1:M}) \prod_{t=1}^T p(\mathbf{y}_t | \mathbf{x}_t) p(\mathbf{x}_t | \tilde{\mathbf{f}}_t). \quad (19)$$

Similarly, we can sample from the TGPSSM prior by first generating a random instance \mathbf{U} from $p(\mathbf{U})$, and then sample \mathbf{f}_t from the conditional distribution $p(\mathbf{f}_t | \mathbf{U}, \mathbf{x}_{t-1})$ at each time step t , given the sampled \mathbf{U} and previous state. The detailed sampling procedure for this prior is given in Appx. A. With the aid of the sparse GP, the computational complexity of the TGPSSM now can be reduced to $\mathcal{O}(d_x T M^2)$ with $M \ll T$, instead of original $\mathcal{O}(d_x T^3)$.

Lastly, we note that if M is sufficiently large, the inducing point \mathbf{U} is often regarded as a *sufficient statistic* for the GP function values \mathbf{F} , in a sense that given \mathbf{U} , the function values \mathbf{F} and any \mathbf{f}_* are independent [42], i.e., $p(\mathbf{f}_* | \mathbf{F}, \mathbf{U}) = p(\mathbf{f}_* | \mathbf{U})$, for any \mathbf{f}_* . This property remains true in the TGP due to the bijective normalizing flow. We summarize the result in the following theorem.

Theorem 2. *If the inducing point, \mathbf{U} , is a sufficient statistic for the standard GP model, meaning that M is sufficiently large, then the transformed inducing point, $\tilde{\mathbf{U}} = \tilde{f}(\mathbf{z}_{1:M})$, is a sufficient statistic for the TGP function values $\tilde{\mathbf{F}} = \tilde{f}(\mathbf{x}_{1:T})$.*

Proof. See Appx. C. \square

Theorem 2 suggests that the TGPSSM inherits the advantage of sparse representations in GP models, which will be significantly beneficial for designing scalable learning and

inference algorithms for TGPSSM (see Section IV). In practice, the number of inducing points, M , is prefixed based on the computing power we can offer. When M is insufficiently large, TGPSSM should finely optimize the inducing locations \mathbf{Z} , to make the transition function be specified by the behavior in those locations; When M is sufficiently large and $\tilde{\mathbf{U}}$ is sufficient statistic for $\tilde{\mathbf{F}}$, TGPSSM is not sensitive to its inducing locations, so it is optional to optimize the position or not. Note that in high-dimensional state space, M is often insufficient large due to the curse of dimensionality; Thus the inducing locations should be optimized in this case.

IV. VARIATIONAL LEARNING AND INFERENCE

To learn the TGPSSM and simultaneously infer the latent states without significant computational cost, this paper resorts to the sparse representation of TGP and variational approximation methods [20]. In the following, Section IV-A first points out the issues existing in the variational GPSSM literature. To overcome these issues, Section IV-B and Section IV-C detail our proposed variational algorithms for the TGPSSM.

A. Variational Inference and Approximations

Let us consider the TGPSSM augmented by sparse inducing points presented in Eq. (19). In Bayesian statistics, a vital object of learning and inference is the model evidence function $p(\mathbf{Y}|\boldsymbol{\theta})$ [54]. For instance, Bayesian learning typically resorts to maximizing the logarithm of the $p(\mathbf{Y}|\boldsymbol{\theta})$ w.r.t. the model parameters $\boldsymbol{\theta}$, which can automatically trade off between data fit and model complexity, in line with Occam's razor rule [55]. However, $p(\mathbf{Y}|\boldsymbol{\theta})$ is obtained by integrating out all the latent variables $\{\mathbf{X}, \tilde{\mathbf{F}}, \tilde{\mathbf{U}}\}$ in the joint distribution (c.f. Eq. (19)), which is analytically intractable. Thus, the posterior distribution of the latent variables, $p(\mathbf{X}, \tilde{\mathbf{F}}, \tilde{\mathbf{U}}|\mathbf{Y}) = \frac{p(\mathbf{Y}, \mathbf{X}, \tilde{\mathbf{F}}, \tilde{\mathbf{U}})}{p(\mathbf{Y}|\boldsymbol{\theta})}$, cannot be represented in closed-form, either. This intractability issue is addressed in the variational Bayesian methods [20] by assuming a variational distribution, $q(\mathbf{X}, \tilde{\mathbf{F}}, \tilde{\mathbf{U}})$, to approximate the intractable $p(\mathbf{X}, \tilde{\mathbf{F}}, \tilde{\mathbf{U}}|\mathbf{Y})$. With the variational distribution, $q(\mathbf{X}, \tilde{\mathbf{F}}, \tilde{\mathbf{U}})$, it can be shown that the logarithm of the evidence function is lower bounded by the so-called evidence lower bound (ELBO) [55],

$$\log p(\mathbf{Y}|\boldsymbol{\theta}) \geq \text{ELBO} = \mathbb{E}_{q(\mathbf{X}, \tilde{\mathbf{F}}, \tilde{\mathbf{U}})} \left[\log \frac{p(\tilde{\mathbf{F}}, \tilde{\mathbf{U}}, \mathbf{X}, \mathbf{Y})}{q(\mathbf{X}, \tilde{\mathbf{F}}, \tilde{\mathbf{U}})} \right], \quad (20)$$

where the ELBO will serve as a surrogate function to be maximized w.r.t. the model parameters and variational distribution, corresponding to the model learning and inference. The tightness of the ELBO is determined by the closeness

between the variational distribution $q(\mathbf{X}, \tilde{\mathbf{F}}, \tilde{\mathbf{U}})$ and the posterior $p(\mathbf{X}, \tilde{\mathbf{F}}, \tilde{\mathbf{U}}|\mathbf{Y})$, measured by the Kullback-Leibler (KL) divergence [20], $\text{KL}[q(\mathbf{X}, \tilde{\mathbf{F}}, \tilde{\mathbf{U}})||p(\mathbf{X}, \tilde{\mathbf{F}}, \tilde{\mathbf{U}}|\mathbf{Y})]$.

The variational distribution needs to be carefully designed. At a high level, it should be flexible enough to closely match $p(\mathbf{X}, \tilde{\mathbf{F}}, \tilde{\mathbf{U}}|\mathbf{Y})$ thus tightening the ELBO, and meanwhile it should be able to make the ELBO more tractable for the downstream optimization problem. Theoretically, the posterior distribution $p(\mathbf{X}, \tilde{\mathbf{F}}, \tilde{\mathbf{U}}|\mathbf{Y})$ should be factorized as

$$p(\tilde{\mathbf{F}}|\tilde{\mathbf{U}}, \mathbf{Y})p(\tilde{\mathbf{U}}|\mathbf{Y})p(\mathbf{x}_0|\mathbf{Y})\prod_{t=1}^T p(\mathbf{x}_t|\tilde{\mathbf{f}}_t, \mathbf{Y}), \quad (21)$$

according to the model defined in Eq. (19). Therefore, the ideal variational distribution for the TGPSSM should similarly be factorized into

$$q(\mathbf{X}, \tilde{\mathbf{F}}, \tilde{\mathbf{U}}) = q(\tilde{\mathbf{F}}|\tilde{\mathbf{U}})q(\tilde{\mathbf{U}})q(\mathbf{x}_0)\prod_{t=1}^T q(\mathbf{x}_t|\tilde{\mathbf{f}}_t), \quad (22)$$

where $q(\tilde{\mathbf{F}}|\tilde{\mathbf{U}})$, $q(\tilde{\mathbf{U}})$, $q(\mathbf{x}_0)$ and $q(\mathbf{x}_t|\tilde{\mathbf{f}}_t)$ are the corresponding variational distributions. The generic factorization of $q(\mathbf{X}, \tilde{\mathbf{F}}, \tilde{\mathbf{U}})$ in Eq. (22) is known as the non-mean-field (NMF) assumption in the GPSSM literature, because it explicitly builds the dependence between latent states and the transition function values. However, the NMF assumption can significantly increase the computational cost for the learning and inference [16]–[18], compared to the mean-field approximation that is summarized as the following:

Assumption 1 (Mean-field assumption). *We assume that the transition function values, $\tilde{\mathbf{f}}_{1:T}$, and the latent states, $\mathbf{x}_{0:T}$, are independent in the variational distribution, i.e., assuming*

$$q(\mathbf{x}_0)\prod_{t=1}^T q(\mathbf{x}_t|\tilde{\mathbf{f}}_t) = q(\mathbf{x}_{0:T}), \quad (23)$$

leading to the corresponding mean-field (MF) variational learning and inference algorithm (see Section IV-B).

Note that the MF assumption simplifies the variational distribution yet enables us to handle a more tractable ELBO [14]. We leave the low-complexity while high-performance NMF variational algorithms for future work.

The existing MF variational inference algorithms in the GPSSM literature [11]–[14] cannot be directly applied to the TGPSSM. For example, to make use of the algorithm in [11], one has to be able to analytically marginalize out the GP transition function values. However, the nonlinear normalizing flow in TGPSSM makes it difficult and even impossible to analytically integrate out the corresponding TGP function values (see Remark 6 in Appx. D). Furthermore, the existing works, e.g. [13], [14], directly assume that $q(\mathbf{x}_{0:T})$ is a joint Gaussian distribution with a Markovian structure, which can fail to closely match the posterior distribution of the latent states that can be neither Gaussian nor unimodal. Another issue is that the existing algorithms overemphasized their capacity of achieving high ELBO value, rather than seeking to learn the informative latent state space representations. As a result, the underlying system dynamics can not be well captured,

leading to degenerated model inference performance. To learn an informative state space representation, one must ensure that the learned state representation can reconstruct the observations and, at the same time, the transition function can characterize the state dynamics [7]. In the following subsections, we propose our variational algorithm to address the aforementioned issues. By explicitly assuming a non-Gaussian variational distribution and exploiting a constrained optimization framework, the proposed algorithm facilitates the improvement of the inference and state-space representation capacities.

B. Mean-Field Variational Algorithm

By applying the same algebraic tricks as in the variational sparse GP [42], i.e., setting $q(\tilde{\mathbf{F}}|\tilde{\mathbf{U}}) = p(\tilde{\mathbf{F}}|\tilde{\mathbf{U}})$, and adopting Assumption 1, the generic variational distribution in Eq. (22) then becomes

$$\begin{aligned} q(\mathbf{X}, \tilde{\mathbf{F}}, \tilde{\mathbf{U}}) &= q(\mathbf{x}_{0:T})q(\tilde{\mathbf{U}})p(\tilde{\mathbf{F}}|\tilde{\mathbf{U}}) \\ &= q(\mathbf{x}_{0:T}) \cdot q(\mathbf{U})\mathbf{J}_{\mathbf{u}} \cdot p(\mathbf{F}|\mathbf{U})\mathbf{J}_{\mathbf{f}}, \end{aligned} \quad (24)$$

where the variational distribution of the inducing points $q(\mathbf{U})$ is assumed to be free-form Gaussian, i.e.,

$$q(\mathbf{U}) = \prod_{d=1}^{d_x} \mathcal{N}(\{\mathbf{u}_{i,d}\}_{i=1}^M | \mathbf{m}_d, \mathbf{L}_d \mathbf{L}_d^\top) = \mathcal{N}(\mathbf{U} | \mathbf{m}, \mathbf{S}), \quad (25)$$

with free variational parameters $\mathbf{m} = [\mathbf{m}_1^\top, \dots, \mathbf{m}_{d_x}^\top]^\top \in \mathbb{R}^{M d_x}$ and $\mathbf{S} = \text{diag}(\mathbf{L}_1 \mathbf{L}_1^\top, \dots, \mathbf{L}_{d_x} \mathbf{L}_{d_x}^\top) \in \mathbb{R}^{M d_x \times M d_x}$. The variational distribution of the latent states, $q(\mathbf{x}_{0:T})$, is assumed to be Markov-structured, and is parameterized by a neural network, a.k.a. inference network, hence the number of variational parameters will not grow linearly with the length of the observation sequence [6]. More specifically, the structured variational distribution is characterized by the following equations,

$$q(\mathbf{x}_0) = \mathcal{N}(\mathbf{x}_0 | \mathbf{m}_0, \mathbf{L}_0 \mathbf{L}_0^\top) \quad (26a)$$

$$q(\mathbf{x}_{0:T}) = q(\mathbf{x}_0) \prod_{t=1}^T q(\mathbf{x}_t | \mathbf{x}_{t-1}) \quad (26b)$$

$$q(\mathbf{x}_t | \mathbf{x}_{t-1}) = \mathcal{N}(\mathbf{x}_t | \boldsymbol{\omega}_\phi(\mathbf{x}_{t-1}, \mathbf{y}_{1:T}), \boldsymbol{\Sigma}_\phi(\mathbf{x}_{t-1}, \mathbf{y}_{1:T})) \quad (26c)$$

where $\boldsymbol{\omega}_\phi(\cdot)$ and $\boldsymbol{\Sigma}_\phi(\cdot)$ are the outputs of the inference network with inputs \mathbf{x}_{t-1} and $\mathbf{y}_{1:T}$, and ϕ denotes the network model parameters; Vector $\mathbf{m}_0 \in \mathbb{R}^{d_x}$ and lower-triangular matrix $\mathbf{L}_0 \in \mathbb{R}^{d_x \times d_x}$ are free variational parameters of $q(\mathbf{x}_0)$. Note that the Markovian structure of $q(\mathbf{x}_{0:T})$ is assumed here as a result of Proposition 1, of which the proof can be found in Appx. D.

Proposition 1. *The optimal state distribution $q^*(\mathbf{x}_{0:T})$ for maximizing the ELBO in the MF case is Markov-structured.*

Remark 2. *Unlike the work in [13], [14] assuming that $q(\mathbf{x}_{0:T})$ is a joint Gaussian distribution with Markovian structure, the variational distribution $q(\mathbf{x}_{0:T})$ defined in Eq. (26) can be non-Gaussian because of the flexibility of the inference network, making the variational distribution more flexible to closely match the possible multimodal posterior distribution of the latent states. It is also worth noting that unlike previous*

Algorithm 1: MF Variational Learning for TGPSSM

Input: Dataset $\mathcal{D}=\{\mathbf{y}_{1:T}\}$; Initial parameters $\boldsymbol{\theta}^{(0)}, \zeta^{(0)}$.
Output: Model parameters $\boldsymbol{\theta}$, variational parameters ζ
while not converged do
 Evaluate Eqs. (27a) and (27b);
 Sample state trajectory $\mathbf{x}_{0:T} \sim q(\mathbf{x}_{0:T})$ (Eq. (26));
 for $t = 1 : T$ **do**
 Evaluate data reconstruction, Eq. (27e), at step t ;
 Evaluate entropy term, Eq. (27c) at step t ;
 Compute $q(\mathbf{f}_t)$ using Eq. (29);
 Sample $\mathbf{f}_t^{(i)} \sim q(\mathbf{f}_t), i = 1, 2, \dots, n$;
 Evaluate state reconstruction, Eq. (28), at step t ;
 end
 Evaluate ELBO of Eq. (27);
 Estimate the Monte-Carlo gradient w.r.t. $\boldsymbol{\theta}$ and ζ ;
 Update $\boldsymbol{\theta}$ and ζ using Adam [57];
end

work in [56] that considers a full factorization over $q(\mathbf{x}_{0:T})$, i.e., $q(\mathbf{x}_{0:T}) = \prod_{t=0}^T q(\mathbf{x}_t)$, in this paper, we analyze the structure of the optimal distribution $q^*(\mathbf{x}_{0:T})$, and maintain the optimal structure for the variational distribution $q(\mathbf{x}_{0:T})$.

Eventually, based on the model defined in Eq. (19) and the variational distributions, we can obtain the corresponding ELBO, which is summarized in the following theorem.

Theorem 3 (Evidence lower bound). *Under Assumption 1, and the variational distributions in Eqs. (24, 25, 26), the ELBO of the TGPSSM defined in Eq. (19) is given by*

ELBO =

$$- \text{KL} [q(\mathbf{x}_0) \| p(\mathbf{x}_0)] \quad (27a)$$

$$- \text{KL} [q(\mathbf{U}) \| p(\mathbf{U})] \quad (27b)$$

$$+ \sum_{t=1}^T \mathbb{E}_{q(\mathbf{x}_{t-1})} \left[\frac{d_x}{2} \log(2\pi) + \frac{1}{2} \log |\boldsymbol{\Sigma}_{\mathbf{x}_t}| + \frac{1}{2} d_x \right] \quad (27c)$$

$$+ \sum_{t=1}^T \mathbb{E}_{q(\mathbf{x}_{t-1:t}, \mathbf{f}_t)} [\log p(\mathbf{x}_t | \mathbb{G}_{\boldsymbol{\theta}_F}(\mathbf{f}_t))] \quad (27d)$$

$$+ \sum_{t=1}^T \mathbb{E}_{q(\mathbf{x}_{t-1})} \left[\log \mathcal{N}(\mathbf{y}_t | \mathbf{C}\boldsymbol{\omega}_{\mathbf{x}_t}, \mathbf{R}) - \frac{1}{2} \text{tr} [\mathbf{R}^{-1}(\mathbf{C}\boldsymbol{\Sigma}_{\mathbf{x}_t}\mathbf{C}^\top)] \right] \quad (27e)$$

where $\boldsymbol{\omega}_{\mathbf{x}_t} \triangleq \boldsymbol{\omega}_\phi(\mathbf{x}_{t-1}, \mathbf{y}_{1:T})$ and $\boldsymbol{\Sigma}_{\mathbf{x}_t} \triangleq \boldsymbol{\Sigma}_\phi(\mathbf{x}_{t-1}, \mathbf{y}_{1:T})$, for notation brevity.

Proof. See Appx. D. \square

Remark 3 (Interpretability of ELBO). *Each subterm in the ELBO in Theorem 3 is interpretable.*

- The KL term in Eq. (27a) represents a regularization term for $q(\mathbf{x}_0)$, which encourages $q(\mathbf{x}_0)$ not staying too “far away” from $p(\mathbf{x}_0) = \mathcal{N}(\mathbf{x}_0 | \mathbf{0}, \mathbf{I})$;
- Eq. (27b) represents a regularization term for the GP transition surrogate $q(\mathbf{U})$, which encourages $q(\mathbf{U})$ not staying too “far away” from the GP prior $p(\mathbf{U})$;
- Eq. (27c) is the differential entropy term of the latent state trajectory. Maximizing the ELBO essentially encourages

“stretching” every $q(\mathbf{x}_t)$ so that the approximated posterior distribution $q(\mathbf{x}_{0:T})$ will not be overly tight;

- Eq. (27d) represents the reconstruction of the latent state trajectory, which encourages the transition function $\mathbb{G}_{\boldsymbol{\theta}_F}(\mathbf{f}_t)$ to fit the latent states $\mathbf{x}_t \sim q(\mathbf{x}_t | \mathbf{x}_{t-1})$. In other words, this term measures the quality of learning/fitting the underlying dynamical functions. Empowered by the normalizing flow, the transition function in TGPSSM is expected to capture more complex state dynamics;
- Eq. (27e) represents the data reconstruction error, which encourages any state trajectory $\mathbf{x}_{0:T}$ from $q(\mathbf{x}_{0:T})$ accurately reconstructing the observations.

Note that there is no analytical form for the calculation of Eq. (27d), we thus use the following approximation instead,

$$\begin{aligned} \text{Eq. (27d)} &\approx \sum_{t=1}^T \mathbb{E}_{q(\mathbf{x}_{t-1:t})} \left[\frac{1}{n} \sum_{i=1}^n \log p(\mathbf{x}_t | \mathbb{G}_{\boldsymbol{\theta}_F}(\mathbf{f}_t^{(i)})) \right] \\ &= \sum_{t=1}^T \mathbb{E}_{q(\mathbf{x}_{t-1:t})} \left[\frac{1}{n} \sum_{i=1}^n \log \mathcal{N}(\mathbf{x}_t | \mathbb{G}_{\boldsymbol{\theta}_F}(\mathbf{f}_t^{(i)}), \mathbf{Q}) \right], \quad (28) \end{aligned}$$

where $\{\mathbf{f}_t^{(i)}\}_{i=1}^n, n \in \mathbb{N}$, are generated from $q(\mathbf{f}_t)$, and

$$q(\mathbf{f}_t) = \int_{\mathbf{U}} q(\mathbf{f}_t, \mathbf{U}) d\mathbf{U} = \mathcal{N}(\mathbf{f}_t | \mathbf{m}_{\mathbf{f}_t}, \boldsymbol{\Sigma}_{\mathbf{f}_t}), \quad (29)$$

and, with a bit abuse of notation,

$$\begin{cases} \mathbf{m}_{\mathbf{f}_t} = K_{\mathbf{x}_{t-1}, \mathbf{z}} K_{\mathbf{z}, \mathbf{z}}^{-1} \mathbf{m}, \\ \boldsymbol{\Sigma}_{\mathbf{f}_t} = K_{\mathbf{x}_{t-1}, \mathbf{x}_{t-1}} - K_{\mathbf{x}_{t-1}, \mathbf{z}} K_{\mathbf{z}, \mathbf{z}}^{-1} [K_{\mathbf{z}, \mathbf{z}} - \mathbf{S}] K_{\mathbf{z}, \mathbf{z}}^{-1} K_{\mathbf{z}, \mathbf{x}_{t-1}}. \end{cases}$$

Lastly, we use the reparametrization trick [58] to compute the expectations w.r.t. the intractable $q(\mathbf{x}_t)$. By sampling trajectories from $q(\mathbf{x}_{0:T})$ and evaluating the integrands in Eq. (27), we can obtain an unbiased estimate of the ELBO. Together with all, we can apply gradient ascent based methods [57] to maximize the ELBO w.r.t. the model parameters $\boldsymbol{\theta} = [\boldsymbol{\theta}_{gp}, \boldsymbol{\theta}_F, \mathbf{Q}, \mathbf{R}]$ and the variational parameters $\zeta = [\mathbf{m}_0, \mathbf{L}_0, \phi, \mathbf{m}, \mathbf{S}, \mathbf{Z}]$. The gradient can be propagated back through time owing to the reparametrization trick [58]. The pseudo code for implementing the MF variational learning and inference algorithm is summarized in Algorithm 1.

Remark 4. *The computational complexity of Algorithm 1 lies in the computations of GP, normalizing flow, and inference network. Compared to the $\mathcal{O}(Td_x M^2)$ computational costs in the GPSSMs using inference networks [14], [16], [17] (if the GP dominates the computational complexity), Algorithm 1 for the TGPSSM only gently increases the computational complexity in the normalizing flow. Especially in the case of applying the elementary flows, the additional computational complexity it brings is almost negligible.*

C. Taming TGPSSM with Constrained Optimization

Algorithm 1 jointly optimizes the parameters $\boldsymbol{\theta}$ and ζ . However, a local optimal with high ELBO (likelihood) does not necessarily imply that the model has learned informative latent state space representations of the underlying system [59]. Similar works in the area of variational autoencode (VAE) address this issue by introducing heuristic weighting

schedules, e.g., β -VAEs [60] where hand-crafted annealing of KL-terms is often used to achieve the desired performance. However, such solutions are not robust to changes in model architecture or dataset [61]. Another line of work resorts to the constrained optimization framework that reformulate the VAE objective function as the Lagrangian of a constrained optimization problem [61]. Inspired by this line of work, we transfer the idea to our TGPSSM and propose a constrained optimization framework to learn more informative state space representations and underlying system dynamics.

For ease of discussion in the sequel, we denote the data reconstruction term, $\sum_{t=1}^T \mathbb{E}_{q(\mathbf{x}_t)} [\log p(\mathbf{y}_t | \mathbf{x}_t)]$ (Eq. (27e) in the ELBO), as \mathcal{R} . To learn a good state space representation that is able to reconstruct the observed data $\mathbf{y}_{1:T}$, we add an additional constraint on \mathcal{R} to control the state space learning behavior. More specifically, we solve the following constrained optimization problem:

$$\min_{\theta, \zeta} -\text{ELBO}, \quad \text{s.t. } \mathcal{R} \geq \mathcal{R}_0, \quad (30)$$

where \mathcal{R}_0 is the desired observation reconstruction quality. Note that compared to the unconstrained optimization $\max_{\theta, \zeta} \text{ELBO}$ solved by Algorithm 1, the constrained optimization problem formulated in Eq. (30) can be interpreted as narrowing down the solution space of $\{\theta, \zeta\}$ by the additional constraint on the data reconstruction term. Thus, the resulting ELBO is guaranteed to be the valid lower bound of the model evidence.

The problem can be solved by using a standard method of Lagrange multipliers, where we introduce the Lagrange multiplier $\beta \geq 0$, and the corresponding Lagrangian \mathcal{L}_β is optimized via a min-max optimization scheme

$$\min_{\theta, \zeta} \max_{\beta \geq 0} \mathcal{L}_\beta = -\text{ELBO} + \beta(\mathcal{R}_0 - \mathcal{R}). \quad (31)$$

The parameters (θ, ζ) are optimized through gradient descent while the Lagrange multiplier β is updated by

$$\beta^{(i)} \leftarrow \beta^{(i-1)} \cdot \exp\left(-\eta \cdot (\hat{\mathcal{R}}^{(i)} - \mathcal{R}_0)\right) \quad (32)$$

to enforce a non-negative β , where η is the associated learning rate and $\hat{\mathcal{R}}^{(i)}$ is an estimate of the data reconstruction term in the i -th iteration. In the context of the stochastic gradient training, $\hat{\mathcal{R}}^{(i)}$ is estimated using moving average, i.e., $\hat{\mathcal{R}}^{(i)} = (1 - \alpha) \cdot \hat{\mathcal{R}}_{batch}^{(i)} + \alpha \cdot \hat{\mathcal{R}}^{(i-1)}$, where α is a prefixed hyperparameter, and $\hat{\mathcal{R}}_{batch}^{(i)}$ is the reconstruction term estimate using current batch data. Throughout this paper, we find that setting the values of $\alpha = 0.5$ and $\eta = 0.001$ can consistently yield a good model performance. For clarity, we summarize the pseudo code for implementing the learning algorithm with constrained optimization framework in Algorithm 2. It is obvious that Algorithm 2 admits the same computational complexity as Algorithm 1.

Remark 5. *Instead of manually tweaking abstract hyperparameter β that implicitly affects the model performance like β -VAEs, Algorithm 2 explicitly adds an additional constraint and updates β in a principled way. Moreover, unlike the constrained optimization problem modeled in VAEs [61] that requires $0 \leq \beta \leq 1$ to guarantee a valid lower bound of the*

Algorithm 2: Taming Variational TGPSSM with Constrained Optimization

Input: Dataset $\mathcal{D}=\{\mathbf{y}_{1:T}\}$; Initial parameters $\theta^{(0)}, \zeta^{(0)}, \beta^{(0)} = 1, i = 0, \alpha = 0.5, \eta = 0.001$.

Output: Model parameters θ , variational parameters ζ
while not converged do

 Estimate $\hat{\mathcal{R}}_{batch}^{(i)}$ (Eq.(27e)) using current batch data;

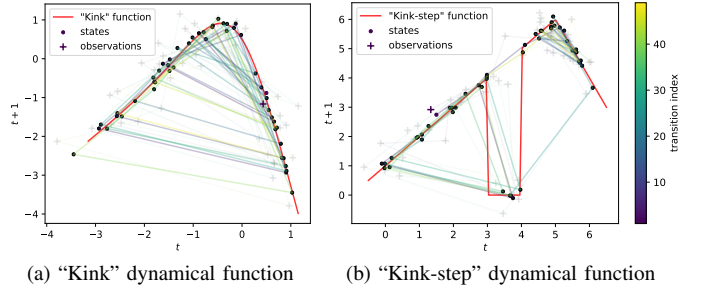
 Estimate $\hat{\mathcal{R}}^{(i)} = (1 - \alpha) \cdot \hat{\mathcal{R}}_{batch}^{(i)} + \alpha \cdot \hat{\mathcal{R}}^{(i-1)}$;

 Update $\beta^{(i)} \leftarrow \beta^{(i-1)} \cdot \exp[-\eta \cdot (\mathcal{R}^{(i)} - \mathcal{R}_0)]$;

 Optimize \mathcal{L}_β w.r.t. θ, ζ as shown in Algorithm 1;

$i \leftarrow i + 1$;

end



(a) “Kink” dynamical function (b) “Kink-step” dynamical function
 Fig. 4: Two 1-D dynamical systems, and the generated 50 latent states & observations.

model evidence, our constrained optimization problem does not require the upper bound constraint for β .

V. EXPERIMENTAL RESULTS

In this section we present an extensive numerical study of the proposed TGPSSM, evaluating its performance in multiple datasets and comparing it to various benchmark algorithms. The detailed experimental configurations can be found in Appendix and the accompanying source code¹.

A. Synthetic Dynamical Systems: Learning the Dynamics

This subsection aims to demonstrate the superior learning performance of TGPSSM on the two 1-D synthetic datasets, namely the *kink* function dataset and the *kink-step* function dataset. Details about the two datasets are listed as follows.

1) **Kink function dataset:** This dataset is generated from a dynamical system that is described by Eq. (33)

$$\mathbf{x}_{t+1} = \underbrace{0.8 + (\mathbf{x}_t + 0.2) \left[1 - \frac{5}{1 + \exp(-2\mathbf{x}_t)} \right]}_{\triangleq \text{“kink function” } f(\mathbf{x}_t)} + \mathbf{v}_t \quad (33a)$$

$$\mathbf{y}_t = \mathbf{x}_t + \mathbf{e}_t, \quad \mathbf{v}_t \sim \mathcal{N}(0, 0.01), \quad \mathbf{e}_t \sim \mathcal{N}(0, 0.1) \quad (33b)$$

where the nonlinear, smooth and time-invariant transition function $f(\mathbf{x}_t)$ is called “kink” function, as depicted in Fig. 4a and Fig. 8a in Appx. K. Note that this test dynamical system has been widely used in the GPSSM literature to show the performance of the learned GP transition posterior [18].

¹Available online: <https://github.com/zhidilin/TGPSSM>

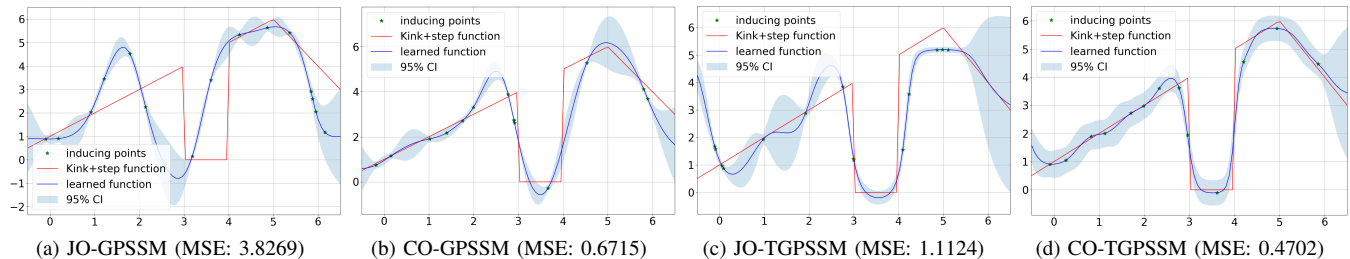


Fig. 5: Learning the “kink-step” dynamical system using GPSSMs and TGPSSMs.

TABLE II: Dynamics learning results of different probabilistic SSMs (MSE)

Model	“Kink” function	“Kink-step” function
BS-GPSSM	0.1068	2.8364
JO-GPSSM	0.0364	3.8269
CO-GPSSM	0.0410	0.6715
PRSSM	1.5605	3.4517
ODGPSSM	1.8431	3.2610
JO-TGPSSM	0.0361	1.1124
CO-TGPSSM	0.0338	0.4702

2) *Kink-step function dataset*: Similar to the kink function dataset, we generate the kink-step function dataset from a modified test dynamical system where the nonlinear time-invariant transition function is a non-smooth piecewise function with both step function and kink function, as described by the following equations and depicted in Fig. 4b and Fig. 8b in Appx. K,

$$\mathbf{x}_{t+1} = \begin{cases} \mathbf{x}_t + 1 + \mathbf{v}_t, & \text{if } \mathbf{x}_t < 3 \text{ or } 4 \leq \mathbf{x}_t < 5 \\ 0 + \mathbf{v}_t, & \text{if } 3 \leq \mathbf{x}_t < 4 \\ 16 - 2\mathbf{x}_t + \mathbf{v}_t, & \text{if } \mathbf{x}_t \geq 5 \end{cases} \quad (34a)$$

$$\mathbf{y}_t = \mathbf{x}_t + \mathbf{e}_t, \quad \mathbf{v}_t \sim \mathcal{N}(0, 0.01), \quad \mathbf{e}_t \sim \mathcal{N}(0, 0.1). \quad (34b)$$

Such modification is for the purpose of testing the performance of the proposed TGPSSMs when there are complex/sharp transitions in the underlying dynamics.

For both test dynamical systems, we independently generate 30 sequences of length $T = 20$ noisy observations \mathbf{y}_t to train the following SSMs.

- **JO-TGPSSM**: The TGPSSM trained using the joint optimization (JO) framework (cf. Algorithm 1)
- **CO-TGPSSM**: The TGPSSM trained using the constrained optimization (CO) framework (cf. Algorithm 2)

We compare our TGPSSMs with the following competitors:

- **BS-GPSSM**: The GPSSM baseline with a Gaussian variational distribution for the latent states [13], [14].
- **JO-GPSSM**: The GPSSM with non-Gaussian variational distribution for the latent states, corresponds to the JO-TGPSSM without using normalizing flow in the transition function modeling.
- **CO-GPSSM**: The GPSSM with non-Gaussian variational distribution for the latent states and trained using the constrained optimization framework, corresponds to the CO-TGPSSM without using normalizing flow in the transition function modeling.
- **PRSSM**: The GPSSM trained using NMF variational algorithm [15].

- **ODGPSSM**: The output-dependent GPSSM trained using NMF learning algorithm [19].

For all models, the size of the inducing points is set to be 15, and the GP model is equipped with the standard SE kernel. For TGPSSMs, we use the normalizing flow concatenating 3 SAL flows with 1 Tanh flow (see Table I), which only involves 16 additional flow parameters (more results of TGPSSM using different flows are presented in Appx. K). For JO-TGPSSM and JO-GPSSM, we found that heuristically setting $\beta = \frac{1}{T}$ as the annealing of the KL-terms help achieve better performance. All the models are trained using the full gradient and the same amount of training epochs (1500 epochs). More experimental configurations can be found in the accompanying source code. Next, we will show a couple of ablation studies.

TGPSSMs vs GPSSMs. Table II (and Fig. 9 in Appx. K) reports the latent transition function learning performance for different SSMs in terms of the data fitting mean-squared error (MSE). It can be observed that both TGPSSMs and GPSSMs (except for PRSSM and ODGPSSM) work well on the kink function dataset, as the underlying dynamic function is differentiable and smooth (cf. Fig. 4a), thus is not difficult to be represented by the standard GP model. However, when it comes to the case of the kink-step function, most GPSSMs fail to capture the underlying complex/sharp dynamics. In contrast, the TGPSSMs consistently outperform the corresponding GPSSMs due to the transformation merits of normalizing flow, see the illustrative results of JO-TGPSSM and CO-TGPSSM, as well as the corresponding GPSSMs depicted in Fig. 5. If we dig a little deeper, there is much more to it, as revealed in Fig. 6. The normalizing flow in the TGPSSM actually can automatically transform the standard GP model to fit the complex kink-step function in a non-linear way; When the underlying system dynamics are simple, e.g., the differentiable and smooth kink function, the normalizing flow in the TGP tends to be an affine transformation, letting the standard GP dominate the modeling procedure. These results empirically verify that the TGPSSM is a unified framework for the GPSSM.

The reason why the GPSSMs with NMF algorithms (PRSSM and ODGPSSM) perform consistently poorly is that the models trained using the NMF algorithms usually require more training epochs. E.g., the NMF algorithm proposed in [16] is reported to have consumed more than 30000 training epochs for the GPSSM to converge when applied to the kink function dataset. Moreover, the NMF algorithms need to carefully initialize the model parameters, making the model training more difficult [18]. In contrast, the TGPSSMs based on the MF algorithm

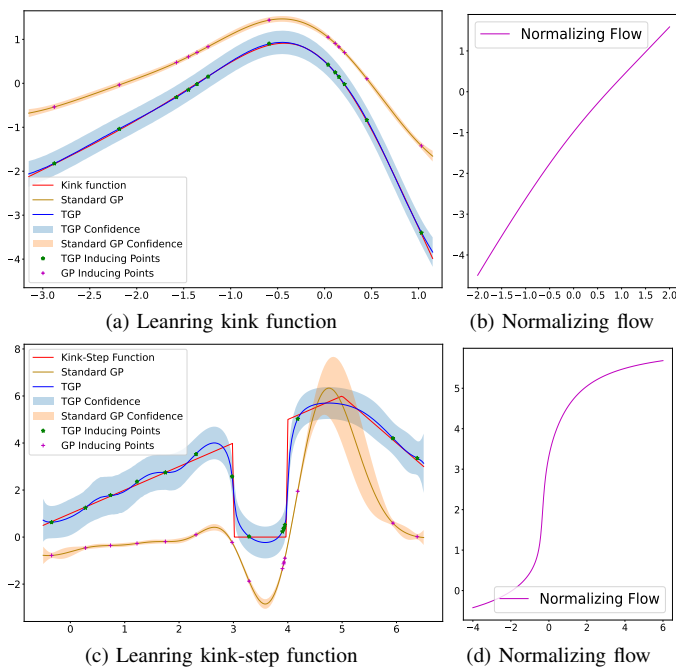


Fig. 6: Details of the TGP posterior for the two transition functions

require simple parameters initialization and achieve the desired performance by only using 1500 training epochs, demonstrating that the superiority of the proposed TGPSSMs in terms of training and learning performance.

Constrained Optimization vs Joint Optimization. By comparing the performance of JO-GPSSM and CO-GPSSM, and that of JO-TGPSSM and CO-TGPSSM from Table II and Fig. 5, we found that the algorithms with the constrained optimization framework consistently outperform the ones using the joint optimization. More concretely, as depicted in Fig. 5a, by using the joint optimization framework, the JO-GPSSM gets stuck into bad local optimal in the learning phase. Thus the learned latent dynamic does not match the underlying one. In contrast, the CO-GPSSM learns a reasonable representation of the underlying system dynamics, as shown in Fig. 5b, even though it still fails to capture the flat and the sharp regions due to the limitations of the standard GP modeling using SE kernel. This demonstrates the capabilities of the CO-GPSSM to construct an informative state-space representation that provides a sound basis for learning the underlying system dynamics. The same conclusion can be drawn from the TGPSSM cases, as depicted in Fig. 5c and Fig. 5d, illustrating the effectiveness of the constrained optimization framework for different models.

Gaussian vs Non-Gaussian. The joint Gaussian variational distribution leads to deteriorated learning performance, as can be observed by comparing the performance of the BS-GPSSM and the JO-GPSSM presented in Table II. Utilizing a more flexible, non-Gaussian variational distribution for latent states allows the GPSSMs to construct more informative state space representations for the latent dynamics learning. Although highly flexible state-space representations might lead the training process to a bad local optimum (c.f. the result of JO-GPSSM), such problem can be remedied using the constrained

optimization framework (c.f. the result of CO-GPSSM).

B. System Identification Datasets: Forecasting Series

This subsection demonstrates the series prediction performance of the proposed methods on the five public real-world system identification datasets² which consist of one-dimensional time series of various lengths between 296 and 1024 data points (see Table V in Appx. K1). For comprehensive model comparisons, in addition to the SSMs considered in Section V-A, we also implemented the DSSM³ proposed in [6] and the TGPSSMs using $J = 3$ layers of RealNVP flow (denoted as JO-TGPSSM-NVP and CO-TGPSSM-NVP). We assume that the one-dimensional observations y_t , are governed by four-dimensional latent states $x_t, \forall t$. The goal of SSMs is to make future forecasting/prediction on observation based upon the learned high-dimensional latent states and the corresponding nonlinear dynamics. All the SSMs are trained with standardized datasets, namely the data are normalized to zero mean and unit variance based on the available training data, and the test data are scaled accordingly. For (T)GPSSMs, the number of inducing points is commonly set to be 20, and the GP models are equipped with the standard SE kernel. More experimental settings are detailed in the supplementary material. Table III reports the prediction performance, where the root-mean-square-error (RMSE) results correspond to predicting 20 steps into the future from the end of the training sequence, and the top three performances are indicated in bold.

Table III depicts that, in general, the best forecasting performance of the four categories of models on the five datasets is TGPSSMs, followed by GPSSMs with MF algorithms and NMF algorithms, and the worst one is the DSSM. These results convincingly illustrates that the proposed TGPSSMs benefit from the flexible function prior and the associated sparse variational learning algorithms. We can also observe that the performance of DSSMs whose transition functions are modeled by deep neural networks is not satisfactory, suggesting that the DSSMs are less competitive for small datasets and low data dimensionality. This is within our expectation since deep neural networks adopted by DSSMs typically require big data to tune a large number of parameters and thus perform poorly in the low data regime. On the contrary, thanks to the unique Bayesian feature of the non-parametric GP model, the resulting GPSSM and TGPSSM are more friendly to small datasets.

The results in Table III also show that the TGPSSMs based on RealNVP achieve comparable performance to TGPSSMs based on elementary flow. From the perspective of model flexibility, TGPSSMs built by the more advanced RealNVP will be more flexible and more generic to the dynamical system modeling problems, especially when no prior knowledge of the problems can be provided. But interestingly, in these five real-world system identification datasets, TGPSSMs based on elementary flow perform fairly well, which demonstrates that GP plus simple flow transformations can construct a flexible TGP prior to meet the requirements of the complex dynamical system learning and inference.

²Available online: <https://homes.esat.kuleuven.be/~smc/daisy/daisydata.html>

³Available online: <https://github.com/guxd/deepHMM>

TABLE III: Prediction performance (RMSE) of different models on the system identification datasets (standardized). Mean and standard deviation of the prediction results are shown across five seeds. The top three results are indicated in bold.

Model Description	Model	Actuator	Ballbeam	Drive	Dryer	Gas Furnace
GPSSMs WITH MF ALGORITHM	BS-GPSSM	0.2115 ± 0.0294	1.0025 ± 0.0997	1.0580 ± 0.2941	0.5485 ± 0.0928	0.4329 ± 0.0583
	JO-GPSSM	0.1083 ± 0.0225	0.2851 ± 0.0179	0.9290 ± 0.1591	0.7725 ± 0.1012	0.4301 ± 0.0562
	CO-GPSSM	0.1067 ± 0.0363	0.1897 ± 0.0614	0.9240 ± 0.1096	0.7766 ± 0.1329	0.3718 ± 0.0395
GPSSMs WITH NMF ALGORITHM	PRSSM	0.4973 ± 0.0503	0.6191 ± 0.0478	0.9802 ± 0.1387	1.1783 ± 0.1095	0.6380 ± 0.0384
	ODGPSSM	0.4814 ± 0.0661	0.5922 ± 0.0597	0.9853 ± 0.1660	1.0535 ± 0.1391	0.5072 ± 0.0823
DSSMs	DSSM	1.0498 ± 0.2082	1.2594 ± 0.2463	1.6879 ± 0.2509	1.7298 ± 0.2261	1.6248 ± 0.2044
TGPSSMs (proposed)	JO-TGPSSM	0.1007 ± 0.0591	0.2227 ± 0.0417	0.7708 ± 0.1302	1.5288 ± 0.1400	0.4156 ± 0.0532
	CO-TGPSSM	0.1008 ± 0.0267	0.2371 ± 0.0485	0.8425 ± 0.1146	0.8883 ± 0.0586	0.3757 ± 0.0159
	JO-TGPSSM-NVP	0.1513 ± 0.0394	0.1681 ± 0.0512	0.9103 ± 0.1570	1.1145 ± 0.1322	0.4077 ± 0.0401
	CO-TGPSSM-NVP	0.1366 ± 0.0202	0.1707 ± 0.0134	0.8453 ± 0.1249	0.8266 ± 0.1543	0.3867 ± 0.0383

TABLE IV: State estimation performance (MSE) of different models

Observations	EKF	CO-GPSSM	CO-TGPSSM
0.1012	0.0237	0.0938	0.0895

Lastly, we note that the BS-GPSSM performs the best on the *Dryer* dataset. This suggests that the state pattern in the *Dryer* dataset is more “Gaussian”, thus matches the joint Gaussian variational distribution of latent states. In this case, additionally increasing the model flexibility complicates model training and thus brings degraded model performance. Specifically, the JO-TGPSSM deviates significantly from the performance of the BS-GPSSM. But it is worth noting that in this case, CO-TGPSSM with constrained optimization framework still retains performance, even though it is still slightly inferior to the GPSSMs. This further verifies that the flexible models benefit significantly from the constrained optimization framework in taming model parameters.

C. Lorenz Attractor: State Inference

Finally, we show the state inference performance of the proposed TGPSSM on the three-dimensional Lorenz system [4] that is described as

$$\mathbf{x}_{t+1} = \mathbf{F}(\mathbf{x}_t) \cdot \mathbf{x}_t + \mathbf{v}_t, \quad \mathbf{v}_t \sim \mathcal{N}(\mathbf{0}, 0.0015 \cdot \mathbf{I}_3), \quad (35a)$$

$$\mathbf{y}_t = \mathbf{I}_3 \cdot \mathbf{x}_t + \mathbf{e}_t, \quad \mathbf{e}_t \sim \mathcal{N}(\mathbf{0}, 0.1 \cdot \mathbf{I}_3), \quad (35b)$$

where the definition and computation of the (Jacobian) transition matrix $\mathbf{F}(\mathbf{x}_t)$ can be found in Eq. 20 of [4]. We compare CO-GPSSM and CO-TGPSSM against EKF, because it has been shown in [4] that when model-based filtering algorithms know exactly the discretized Lorenz system information, the EKF can achieve best state inference results. We thus use the EKF as a baseline for the state estimation MSE lower bound. We generate a sequence of the length $T = 2000$ for training the CO-GPSSM and CO-TGPSSM. The state inference results are presented in Table IV and Fig. 10 in Appx. K. It can be found that the state inference performance of (T)GPSSMs is reasonably comparable to the EKF in terms of the state-fitting MSE, given the fact that only noisy measurements are provided for the training of (T)GPSSMs. The results also suggest model knowledge plays a vital role in state estimation. For the data-driven (T)GPSSMs, its learned latent space representation

should fuse model knowledge as possible to gain a better state inference performance, which is left for future exploration.

VI. CONCLUSION

In this paper, a flexible and unified probabilistic state-space model called TGPSSM has been proposed. By leveraging the normalizing flow technique, TGPSSM enlarges the GP priors in standard GPSSM, making the TGPSSM more flexible and expressive to model complex dynamical systems. We also propose a variational learning algorithm (Algorithm 2) that is superior from the perspectives of scalability, flexibility and interpretability to learn the proposed TGPSSM and infer the latent states simultaneously. Experimental results on various test datasets demonstrate that the proposed TGPSSM empowered by the proposed variational learning algorithm can improve complex dynamical system learning and inference performance compared to several state-of-the-art and traditional methods.

REFERENCES

- [1] S. Särkkä, *Bayesian filtering and smoothing*. Cambridge University Press, 2013, no. 3.
- [2] Z. Yan, P. Cheng, Z. Chen, Y. Li, and B. Vucetic, “Gaussian process reinforcement learning for fast opportunistic spectrum access,” *IEEE Trans. Signal Process.*, vol. 68, pp. 2613–2628, Apr. 2020.
- [3] A. M. Alaa and M. van der Schaar, “Attentive state-space modeling of disease progression,” in *Proc. Adv. Neural Inf. Process. Syst. (NeurIPS)*, Vancouver, BC, Canada, Dec. 2019, pp. 11 338–11 348.
- [4] G. Revach, N. Shlezinger, X. Ni, A. L. Escoriza, R. J. Van Sloun, and Y. C. Eldar, “KalmanNet: Neural network aided Kalman filtering for partially known dynamics,” *IEEE Trans. Signal Process.*, vol. 70, pp. 1532–1547, Mar. 2022.
- [5] M. Karl, M. Soelch, J. Bayer, and P. Van der Smagt, “Deep variational Bayes filters: Unsupervised learning of state space models from raw data,” in *Proc. Int. Conf. Learn. Represent. (ICLR)*, Toulon, France, Apr. 2017.
- [6] R. Krishnan, U. Shalit, and D. Sontag, “Structured inference networks for nonlinear state space models,” in *Proc. AAAI Conf. Artif. Intell. (AAAI)*, San Francisco, CA, United states, Feb. 2017, pp. 2101–2109.
- [7] D. Gedon, N. Wahlström, T. B. Schön, and L. Ljung, “Deep state space models for nonlinear system identification,” *IFAC-PapersOnLine*, vol. 54, no. 7, pp. 481–486, 2021.
- [8] R. Turner, M. Deisenroth, and C. Rasmussen, “State-space inference and learning with Gaussian processes,” in *Proc. Int. Conf. Artif. Intell. Stat. (AISTATS)*, Sardinia, Italy, May 2010, pp. 868–875.
- [9] J. Ko and D. Fox, “Learning GP-BayesFilters via Gaussian process latent variable models,” *Auton. Robots*, vol. 30, no. 1, pp. 3–23, Oct. 2011.
- [10] R. Frigola, F. Lindsten, T. B. Schön, and C. E. Rasmussen, “Bayesian inference and learning in Gaussian process state-space models with particle MCMC,” in *Proc. Adv. Neural Inf. Process. Syst. (NeurIPS)*, Lake Tahoe, NV, United states, Dec. 2013, pp. 3156–3164.

- [11] R. Frigola, Y. Chen, and C. E. Rasmussen, "Variational Gaussian process state-space models," in *Proc. Adv. Neural Inf. Process. Syst. (NeurIPS)*, Montreal, QC, Canada, Dec. 2014, pp. 3680–3688.
- [12] R. Frigola, "Bayesian time series learning with Gaussian processes," Ph.D. dissertation, University of Cambridge, 2015.
- [13] A. J. McHutchon, "Nonlinear modelling and control using Gaussian processes," Ph.D. dissertation, University of Cambridge, 2014.
- [14] S. Eleftheriadis, T. Nicholson, M. P. Deisenroth, and J. Hensman, "Identification of Gaussian process state space models," in *Proc. Adv. Neural Inf. Process. Syst. (NeurIPS)*, Long Beach, CA, United states, Dec. 2017, pp. 5309–5319.
- [15] A. Doerr, C. Daniel, M. Schiegg, N.-T. Duy, S. Schaal, M. Toussaint, and T. Sebastian, "Probabilistic recurrent state-space models," in *Proc. Int. Conf. Mach. Learn. (ICML)*, Stockholm, Sweden, Jul. 2018, pp. 1280–1289.
- [16] A. D. Ialongo, M. van der Wilk, J. Hensman, and C. E. Rasmussen, "Overcoming mean-field approximations in recurrent Gaussian process models," in *Proc. Int. Conf. Mach. Learn. (ICML)*, Long Beach, CA, United states, Jun. 2019, pp. 2931–2940.
- [17] S. Curi, S. Melchior, F. Berkenkamp, and A. Krause, "Structured variational inference in partially observable unstable Gaussian process state space models," in *Proc. Learning for Dynamics and Control (LADC)*, Virtual, Online, Jun. 2020, pp. 147–157.
- [18] J. Lindinger, B. Rakitsch, and C. Lippert, "Laplace approximated Gaussian process state-space models," in *Proc. Conf. Uncertain. Artif. Intell. (UAI)*, Eindhoven, Netherlands, Aug. 2022.
- [19] Z. Lin, L. Cheng, F. Yin, L. Xu, and S. Cui, "Output-dependent Gaussian process state-space model," *arXiv preprint arXiv:2212.07608*, 2022.
- [20] S. Theodoridis, *Machine Learning: A Bayesian and Optimization Perspective*, 2nd ed. Academic Press, 2020.
- [21] C. E. Rasmussen and C. K. I. Williams, *Gaussian Processes for Machine Learning*. MIT Press, 2006.
- [22] A. Kullberg, I. Skog, and G. Hendeby, "Online joint state inference and learning of partially unknown state-space models," *IEEE Trans. Signal Process.*, vol. 69, pp. 4149–4161, 2021.
- [23] J. Ko and D. Fox, "GP-BayesFilters: Bayesian filtering using Gaussian process prediction and observation models," *Auton. Robots*, vol. 27, no. 1, pp. 75–90, Jul. 2009.
- [24] M. P. Deisenroth, R. D. Turner, M. F. Huber, U. D. Hanebeck, and C. E. Rasmussen, "Robust filtering and smoothing with Gaussian processes," *IEEE Trans. Autom. Control*, vol. 57, no. 7, pp. 1865–1871, 2011.
- [25] M. P. Deisenroth, D. Fox, and C. E. Rasmussen, "Gaussian processes for data-efficient learning in robotics and control," *IEEE Trans. Pattern Anal. Mach. Intell.*, vol. 37, no. 2, pp. 408–423, 2013.
- [26] J. M. Wang, D. J. Fleet, and A. Hertzmann, "Gaussian process dynamical models for human motion," *IEEE Trans. Pattern Anal. Mach. Intell.*, vol. 30, no. 2, pp. 283–298, 2007.
- [27] Y. Liu and P. M. Djurić, "Gaussian process state-space models with time-varying parameters and inducing points," in *Proc. European Signal Proces. Conf. (EUSIPCO)*, Amsterdam, Netherlands, Jan. 2021, pp. 1462–1466.
- [28] Y. Liu, M. Ajirak, and P. M. Djurić, "Inference with deep Gaussian process state space models," in *Proc. European Signal Proces. Conf. (EUSIPCO)*, Belgrade, Serbia, Oct. 2022, pp. 792–796.
- [29] A. Xie, F. Yin, B. Ai, S. Zhang, and S. Cui, "Learning while tracking: A practical system based on variational Gaussian process state-space model and smartphone sensory data," in *Proc. Int. Conf. Inf. Fusion (FUSION)*, Rustenburg, South Africa, Jul. 2020, pp. 1–7.
- [30] F. Yin, Z. Lin, Q. Kong, Y. Xu, D. Li, S. Theodoridis, and S. R. Cui, "Fedloc: Federated learning framework for data-driven cooperative localization and location data processing," *IEEE Open J. Signal Process.*, vol. 1, pp. 187–215, 2020.
- [31] Y. Zhao, C. Fritsche, G. Hendeby, F. Yin, T. Chen, and F. Gunnarsson, "Cramér–Rao bounds for filtering based on Gaussian process state-space models," *IEEE Trans. Signal Process.*, vol. 67, no. 23, pp. 5936–5951, 2019.
- [32] A. Damianou and N. D. Lawrence, "Deep Gaussian processes," in *Proc. Int. Conf. Artif. Intell. Stat. (AISTATS)*. PMLR, 2013, pp. 207–215.
- [33] G. A. Ríos Díaz, "Contributions to Bayesian machine learning via transport maps," Ph.D. dissertation, University of Chile, 2020.
- [34] J. Maroñas, O. Hamelijnck, J. Knoblauch, and T. Damoulas, "Transforming Gaussian processes with normalizing flows," in *Proc. Int. Conf. Artif. Intell. Stat. (AISTATS)*, Virtual, Online, Apr. 2021, pp. 1081–1089.
- [35] A. Wilson and R. Adams, "Gaussian process kernels for pattern discovery and extrapolation," in *Proc. Int. Conf. Mach. Learn. (ICML)*, Atlanta, GA, United states, Jun. 2013, pp. 1067–1075.
- [36] F. Yin, L. Pan, T. Chen, S. Theodoridis, Z.-Q. T. Luo, and A. M. Zoubir, "Linear multiple low-rank kernel based stationary Gaussian processes regression for time series," *IEEE Trans. Signal Process.*, vol. 68, pp. 5260–5275, 2020.
- [37] R. C. Suwandi, Z. Lin, Y. Sun, Z. Wang, L. Cheng, and F. Yin, "Gaussian process regression with grid spectral mixture kernel: Distributed learning for multidimensional data," in *Proc. Int. Conf. Inf. Fusion (FUSION)*, Linköping, Sweden, July 2022, pp. 1–8.
- [38] A. G. Wilson, Z. Hu, R. Salakhutdinov, and E. P. Xing, "Deep kernel learning," in *Proc. Int. Conf. Artif. Intell. Stat. (AISTATS)*, Cadiz, Spain, May 2016, pp. 370–378.
- [39] Y. Dai, T. Zhang, Z. Lin, F. Yin, S. Theodoridis, and S. Cui, "An interpretable and sample efficient deep kernel for gaussian process," in *Proc. Conf. Uncertain. Artif. Intell. (UAI)*, Virtual, Online, Aug. 2020, pp. 759–768.
- [40] G. Papamakarios, E. Nalisnick, D. J. Rezende, S. Mohamed, and B. Lakshminarayanan, "Normalizing flows for probabilistic modeling and inference," *J. Mach. Learn. Res.*, vol. 22, no. 57, pp. 1–64, Mar. 2021.
- [41] I. Kobyzev, S. J. Prince, and M. A. Brubaker, "Normalizing flows: An introduction and review of current methods," *IEEE Trans. Pattern Anal. Mach. Intell.*, vol. 43, no. 11, pp. 3964–3979, 2020.
- [42] J. Hensman, N. Fusi, and N. D. Lawrence, "Gaussian processes for big data," in *Proc. Conf. Uncertain. Artif. Intell. (UAI)*, 2013, pp. 282–290.
- [43] Z. Chen, J. Fan, and K. Wang, "Remarks on multivariate Gaussian process," *arXiv preprint arXiv:2010.09830*, 2020.
- [44] T. Tao, *An introduction to measure theory*. American Mathematical Society Providence, RI, 2011, vol. 126.
- [45] A. C. Atkinson, M. Riani, and A. Corbellini, "The Box-Cox transformation: Review and extensions," *Statistical Science*, vol. 36, no. 2, pp. 239–255, 2021.
- [46] E. Snelson, Z. Ghahramani, and C. Rasmussen, "Warped Gaussian processes," *Proc. Adv. Neural Inf. Process. Syst. (NeurIPS)*, vol. 16, 2003.
- [47] G. Rios and F. Tobar, "Compositionally-warped Gaussian processes," *Neural Netw.*, vol. 118, pp. 235–246, 2019.
- [48] H. Salimbeni and M. P. Deisenroth, "Doubly stochastic variational inference for deep Gaussian processes," in *Proc. Adv. Neural Inf. Process. Syst. (NeurIPS)*, 2017, pp. 4591–4602.
- [49] A. G. Wilson and Z. Ghahramani, "Copula processes," *Proc. Adv. Neural Inf. Process. Syst. (NeurIPS)*, vol. 23, 2010.
- [50] M. C. Jones and A. Pewsey, "Sinh-arcsinh distributions," *Biometrika*, vol. 96, no. 4, pp. 761–780, 2009.
- [51] L. Dinh and S. Bengio, "Density estimation using Real NVP," in *Proc. Int. Conf. Learn. Represent. (ICLR)*, Toulon, France, Apr. 2017.
- [52] R. T. Chen, Y. Rubanova, J. Bettencourt, and D. K. Duvenaud, "Neural ordinary differential equations," in *Proc. Adv. Neural Inf. Process. Syst. (NeurIPS)*, Montreal, QC, Canada, Dec. 2018, pp. 6572–6583.
- [53] S. Bond-Taylor, A. Leach, Y. Long, and C. G. Willcocks, "Deep generative modelling: A comparative review of VAEs, GANs, normalizing flows, energy-based and autoregressive models," *IEEE Trans. Pattern Anal. Mach. Intell.*, vol. 44, no. 11, pp. 7327–7347, Sep. 2021.
- [54] J. Courts, A. G. Wills, and T. B. Schön, "Gaussian variational state estimation for nonlinear state-space models," *IEEE Trans. Signal Process.*, vol. 69, pp. 5979–5993, Oct. 2021.
- [55] L. Cheng, F. Yin, S. Theodoridis, S. Chatzis, and T.-H. Chang, "Rethinking Bayesian learning for data analysis: The art of prior and inference in sparsity-aware modeling," *IEEE Signal Process. Mag.*, vol. 39, no. 6, pp. 18–52, Nov. 2022.
- [56] C. L. C. Mattos and G. A. Barreto, "A stochastic variational framework for recurrent Gaussian processes models," *Neural Netw.*, vol. 112, pp. 54–72, Apr. 2019.
- [57] D. P. Kingma and J. Ba, "Adam: A method for stochastic optimization," in *Proc. Int. Conf. Learn. Represent. (ICLR)*, San Diego, CA, United states, May 2015.
- [58] D. P. Kingma and M. Welling, "An introduction to variational autoencoders," *Found. Trends Mach. Learn.*, vol. 12, no. 4, pp. 307–392, 2019.
- [59] A. Alemi, B. Poole, I. Fischer, J. Dillon, R. A. Saurous, and K. Murphy, "Fixing a broken ELBO," in *Proc. Int. Conf. Mach. Learn. (ICML)*, Stockholm, Sweden, Jul. 2018, pp. 159–168.
- [60] H. Sikka, W. Zhong, J. Yin, and C. Pehlevant, "A closer look at disentangling in β -VAE," in *Proc. Asilomar Conf. Signals Syst. Comput. (ACSSC)*, Pacific Grove, CA, United states, Nov. 2019, pp. 888–895.
- [61] A. Klushyn, N. Chen, R. Kurlle, B. Cseke, and P. van der Smagt, "Learning hierarchical priors in VAEs," in *Proc. Adv. Neural Inf. Process. Syst. (NeurIPS)*, Vancouver, BC, Canada, Dec. 2019, pp. 2870–2879.

APPENDIX

A. Sampling from TGPSSM

For notational brevity, we only show the sampling steps in the case of one-dimensional hidden state. It can be straightforwardly extended to high-dimensional hidden state cases.

- **TGPSSM:** If $f(\cdot) \sim \mathcal{GP}(0, k(\cdot, \cdot))$, and the marginal flow is $\mathbb{G}(\cdot) : \mathcal{F} \mapsto \mathcal{F}$, then we can sample the entire TGPSSM state trajectory by the following steps:

$$\mathbf{x}_0 \sim p(\mathbf{x}_0), \quad (36a)$$

$$\mathbf{f}_1 | \mathbf{x}_0 \sim \mathcal{N}(\mathbf{f}_1 | \mathbf{0}, \mathbf{K}_{\mathbf{x}_0, \mathbf{x}_0}) \quad (36b)$$

$$\tilde{\mathbf{f}}_1 = \mathbb{G}(\mathbf{f}_1) \quad (36c)$$

$$\mathbf{x}_1 | \tilde{\mathbf{f}}_1 \sim \mathcal{N}(\mathbf{x}_1 | \tilde{\mathbf{f}}_1, \mathbf{Q}) \quad (36d)$$

$$\mathbf{f}_2 | \mathbf{f}_1, \mathbf{x}_{0:1} \sim \mathcal{N}(\mathbf{f}_2 | \mathbf{K}_{\mathbf{x}_1, \mathbf{x}_0} \mathbf{K}_{\mathbf{x}_0, \mathbf{x}_0}^{-1} \mathbf{f}_1, \mathbf{K}_{\mathbf{x}_1, \mathbf{x}_1} - \mathbf{K}_{\mathbf{x}_1, \mathbf{x}_0} \mathbf{K}_{\mathbf{x}_0, \mathbf{x}_0}^{-1} \mathbf{K}_{\mathbf{x}_0, \mathbf{x}_1}) \quad (36e)$$

$$\tilde{\mathbf{f}}_2 = \mathbb{G}(\mathbf{f}_2) \quad (36f)$$

$$\mathbf{x}_2 | \tilde{\mathbf{f}}_2 \sim \mathcal{N}(\mathbf{x}_2 | \tilde{\mathbf{f}}_2, \mathbf{Q}) \quad (36g)$$

$$\mathbf{f}_3 | \mathbf{f}_{1:2}, \mathbf{x}_{0:2} \sim \mathcal{N}(\mathbf{f}_3 | \mathbf{K}_{\mathbf{x}_2, \mathbf{x}_{0:1}} \mathbf{K}_{\mathbf{x}_{0:1}, \mathbf{x}_{0:1}}^{-1} \mathbf{f}_{1:2}, \mathbf{K}_{\mathbf{x}_2, \mathbf{x}_2} - \mathbf{K}_{\mathbf{x}_2, \mathbf{x}_{0:1}} \mathbf{K}_{\mathbf{x}_{0:1}, \mathbf{x}_{0:1}}^{-1} \mathbf{K}_{\mathbf{x}_{0:1}, \mathbf{x}_2}) \quad (36h)$$

$$\tilde{\mathbf{f}}_3 = \mathbb{G}(\mathbf{f}_3) \quad (36i)$$

$$\mathbf{x}_3 | \tilde{\mathbf{f}}_3 \sim \mathcal{N}(\mathbf{x}_3 | \tilde{\mathbf{f}}_3, \mathbf{Q}) \quad (36j)$$

⋮

$$\mathbf{f}_t | \mathbf{f}_{1:t-1}, \mathbf{x}_{0:t-1} \sim \mathcal{N}(\mathbf{f}_t | \mathbf{K}_{\mathbf{x}_{t-1}, \mathbf{x}_{0:t-2}} \mathbf{K}_{\mathbf{x}_{0:t-2}, \mathbf{x}_{0:t-2}}^{-1} \mathbf{f}_{1:t-1}, \mathbf{K}_{\mathbf{x}_{t-1}, \mathbf{x}_{t-1}} - \mathbf{K}_{\mathbf{x}_{t-1}, \mathbf{x}_{0:t-2}} \mathbf{K}_{\mathbf{x}_{0:t-2}, \mathbf{x}_{0:t-2}}^{-1} \mathbf{K}_{\mathbf{x}_{0:t-2}, \mathbf{x}_{t-1}}) \quad (36k)$$

$$\tilde{\mathbf{f}}_t = \mathbb{G}(\mathbf{f}_t) \quad (36l)$$

$$\mathbf{x}_t | \tilde{\mathbf{f}}_t \sim \mathcal{N}(\mathbf{x}_t | \tilde{\mathbf{f}}_t, \mathbf{Q}) \quad (36m)$$

⋮

Note that the GP sampling steps conditioning on previous sampled states guarantee the sampled state trajectory is consistent.

- **Augmented TGPSSM:** In the TGPSSM augmented by sparse inducing points, the set of inducing points \mathbf{U} serves as the surrogate (sufficient statistic) of \mathbf{F} , therefore, the GP transition function value \mathbf{f}_t in each step can be obtained by conditioning on \mathbf{U} , the sampling steps are summarized as follows:

$$\mathbf{U} \sim p(\mathbf{U} | \mathbf{0}, \mathbf{K}_{\mathbf{Z}, \mathbf{Z}}) \quad (37a)$$

$$\mathbf{x}_0 \sim p(\mathbf{x}_0), \quad (37b)$$

$$\mathbf{f}_1 | \mathbf{x}_0, \mathbf{U} \sim \mathcal{N}(\mathbf{f}_1 | \mathbf{K}_{\mathbf{x}_0, \mathbf{Z}} \mathbf{K}_{\mathbf{Z}, \mathbf{Z}}^{-1} \mathbf{U}, \mathbf{K}_{\mathbf{x}_0, \mathbf{x}_0} - \mathbf{K}_{\mathbf{x}_0, \mathbf{Z}} \mathbf{K}_{\mathbf{Z}, \mathbf{Z}}^{-1} \mathbf{K}_{\mathbf{Z}, \mathbf{x}_0}^\top) \quad (37c)$$

$$\tilde{\mathbf{f}}_1 = \mathbb{G}(\mathbf{f}_1) \quad (37d)$$

$$\mathbf{x}_1 | \tilde{\mathbf{f}}_1 \sim \mathcal{N}(\mathbf{x}_1 | \tilde{\mathbf{f}}_1, \mathbf{Q}) \quad (37e)$$

$$\mathbf{f}_2 | \mathbf{x}_1, \mathbf{U} \sim \mathcal{N}(\mathbf{f}_2 | \mathbf{K}_{\mathbf{x}_1, \mathbf{Z}} \mathbf{K}_{\mathbf{Z}, \mathbf{Z}}^{-1} \mathbf{U}, \mathbf{K}_{\mathbf{x}_1, \mathbf{x}_1} - \mathbf{K}_{\mathbf{x}_1, \mathbf{Z}} \mathbf{K}_{\mathbf{Z}, \mathbf{Z}}^{-1} \mathbf{K}_{\mathbf{Z}, \mathbf{x}_1}^\top) \quad (37f)$$

$$\tilde{\mathbf{f}}_2 = \mathbb{G}(\mathbf{f}_2) \quad (37g)$$

$$\mathbf{x}_2 | \tilde{\mathbf{f}}_2 \sim \mathcal{N}(\mathbf{x}_2 | \tilde{\mathbf{f}}_2, \mathbf{Q}) \quad (37h)$$

⋮

$$\mathbf{f}_t | \mathbf{x}_{t-1}, \mathbf{U} \sim \mathcal{N}(\mathbf{f}_t | \mathbf{K}_{\mathbf{x}_{t-1}, \mathbf{Z}} \mathbf{K}_{\mathbf{Z}, \mathbf{Z}}^{-1} \mathbf{U}, \mathbf{K}_{\mathbf{x}_{t-1}, \mathbf{x}_{t-1}} - \mathbf{K}_{\mathbf{x}_{t-1}, \mathbf{Z}} \mathbf{K}_{\mathbf{Z}, \mathbf{Z}}^{-1} \mathbf{K}_{\mathbf{Z}, \mathbf{x}_{t-1}}^\top) \quad (37i)$$

$$\tilde{\mathbf{f}}_t = \mathbb{G}(\mathbf{f}_t) \quad (37j)$$

$$\mathbf{x}_t | \tilde{\mathbf{f}}_t \sim \mathcal{N}(\mathbf{x}_t | \tilde{\mathbf{f}}_t, \mathbf{Q}) \quad (37k)$$

⋮

The comparisons of state trajectory behavior of GPSSM and the corresponding TGPSSM prior are demonstrated in Fig. 7, where the standard SE kernel (with length scale = 2.5, and output scale = 1) is used for both GPSSM and TGPSSM; Furthermore, two SAL layers together with one Tanh flows are used for TGPSSM (see Table I for the details). From Fig. 7, we can, on the

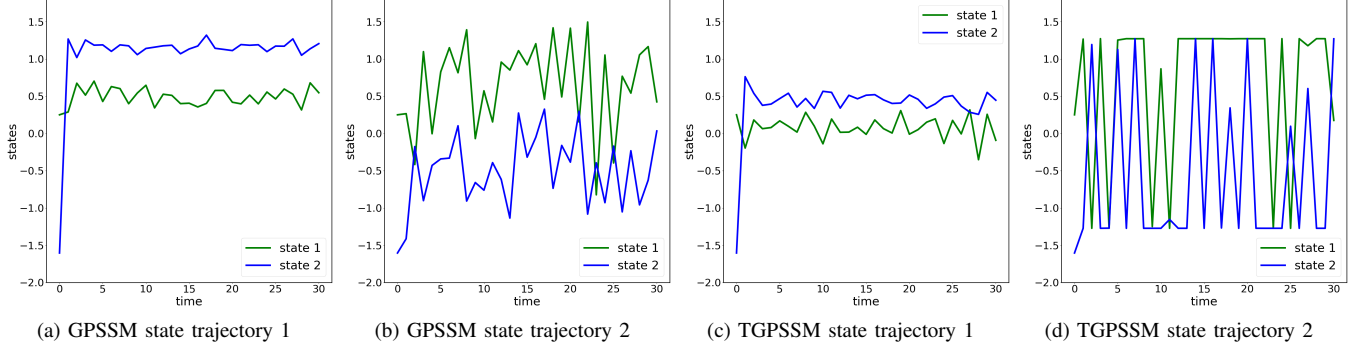


Fig. 7: State trajectories in the 2-dimensional state-space are sampled from a GPSSM prior and the corresponding TGPSSM prior. The kernel function used in GPSSM and TGPSSM is the SE kernel with fixed kernel length-scale and output-scale hyperparameters. The normalizing flows used in TGPSSM are simply a combination of two blocks of SAL flow and one block of Tanh flow. Trajectory example in Panel (c) shows behavior similar to that of the GPSSM (panel (a)); In Panel (d), the trajectory of TGPSSM behaves like sawtooth and square waves, which is unlikely to sample from the GPSSM.

one hand, observe that the TGPSSM prior maintains rich nonlinear dynamics family described by the SE kernel in GPSSM. On the other hand, TGPSSM using normalizing flows brings extra nonlinear dynamics that cannot be represented by the SE kernel. For example, the square wave type state trajectories drawn from TGPSSM, as depicted in Fig. 7(d), are hard to model using standard GP with the SE kernel, due to the continuous and infinitely differentiable function properties in the GP with SE kernel [21].

B. Augmented TGP Prior: Derivation of Eq. (17)

Similar derivations can be found in the literature, e.g. [34]. For ease of reference, we also present the proof here. By definition, it is easy to write down $p(\tilde{\mathbf{F}}, \tilde{\mathbf{U}})$ and $p(\tilde{\mathbf{U}})$,

$$p(\tilde{\mathbf{F}}, \tilde{\mathbf{U}}) = p(\mathbf{F}, \mathbf{U}) \prod_{j=0}^{J-1} \det \left(\begin{array}{c|c} \underbrace{\frac{\partial \mathbb{G}_{\theta_j}(\mathbb{G}_{\theta_{j-1}}(\dots \mathbb{G}_{\theta_0}(\mathbf{F}) \dots))}{\partial \mathbb{G}_{\theta_{j-1}}(\dots \mathbb{G}_{\theta_0}(\mathbf{F}) \dots)}}_A & \underbrace{\frac{\partial \mathbb{G}_{\theta_j}(\mathbb{G}_{\theta_{j-1}}(\dots \mathbb{G}_{\theta_0}(\mathbf{F}) \dots))}{\partial \mathbb{G}_{\theta_{j-1}}(\dots \mathbb{G}_{\theta_0}(\mathbf{U}) \dots)}}_B \\ \hline \underbrace{\frac{\partial \mathbb{G}_{\theta_j}(\mathbb{G}_{\theta_{j-1}}(\dots \mathbb{G}_{\theta_0}(\mathbf{U}) \dots))}{\partial \mathbb{G}_{\theta_{j-1}}(\dots \mathbb{G}_{\theta_0}(\mathbf{F}) \dots)}}_C & \underbrace{\frac{\partial \mathbb{G}_{\theta_j}(\mathbb{G}_{\theta_{j-1}}(\dots \mathbb{G}_{\theta_0}(\mathbf{U}) \dots))}{\partial \mathbb{G}_{\theta_{j-1}}(\dots \mathbb{G}_{\theta_0}(\mathbf{U}) \dots)}}_D \end{array} \right)^{-1}, \quad (38a)$$

$$p(\tilde{\mathbf{U}}) = p(\mathbf{U}) \underbrace{\prod_{j=0}^{J-1} \left| \det \frac{\partial \mathbb{G}_{\theta_j}(\mathbb{G}_{\theta_{j-1}}(\dots \mathbb{G}_{\theta_0}(\mathbf{U}) \dots))}{\partial \mathbb{G}_{\theta_{j-1}}(\dots \mathbb{G}_{\theta_0}(\mathbf{U}) \dots)} \right|^{-1}}_{\mathbf{J}_{\mathbf{u}}}. \quad (38b)$$

Since

$$\begin{cases} p(\tilde{\mathbf{F}} | \tilde{\mathbf{U}}) = \frac{p(\tilde{\mathbf{F}}, \tilde{\mathbf{U}})}{p(\tilde{\mathbf{U}})}, \\ \det \begin{pmatrix} A & B \\ C & D \end{pmatrix} = \det(A - BD^{-1}C) \det(D), \end{cases} \quad (39)$$

by combining Eqs. (38a), (38b) and (39), we have

$$\begin{aligned} p(\tilde{\mathbf{F}} | \tilde{\mathbf{U}}) &= p(\mathbf{F} | \mathbf{U}) \prod_{j=0}^{J-1} |\det(A - BD^{-1}C)|^{-1} \\ &= p(\mathbf{F} | \mathbf{U}) \prod_{j=0}^{J-1} |A|^{-1} \quad (B = 0, C = 0 \text{ in Eq. (38a)}) \\ &= p(\mathbf{F} | \mathbf{U}) \underbrace{\prod_{j=0}^{J-1} \left| \frac{\partial \mathbb{G}_{\theta_j}(\mathbb{G}_{\theta_{j-1}}(\dots \mathbb{G}_{\theta_0}(\mathbf{F}) \dots))}{\partial \mathbb{G}_{\theta_{j-1}}(\dots \mathbb{G}_{\theta_0}(\mathbf{F}) \dots)} \right|^{-1}}_{\mathbf{J}_{\mathbf{f}}}. \end{aligned} \quad (40)$$

Therefore, the augmented TGP prior $p(\mathbf{F}, \mathbf{U})$ is

$$p(\tilde{\mathbf{F}}, \tilde{\mathbf{U}}) = p(\tilde{\mathbf{F}} | \tilde{\mathbf{U}})p(\tilde{\mathbf{U}}) = \underbrace{p(\mathbf{F} | \mathbf{U}) \cdot \mathbf{J}_{\mathbf{f}}}_{p(\tilde{\mathbf{f}}_{1:T} | \tilde{\mathbf{u}}_{1:T})} \cdot \underbrace{p(\mathbf{U}) \cdot \mathbf{J}_{\mathbf{u}}}_{p(\tilde{\mathbf{u}}_{1:T})}. \quad (41)$$

C. Proof of Theorem 2

1) We first show that if \mathbf{U} is sufficient for \mathbf{F} , then \mathbf{U} is sufficient for $\tilde{\mathbf{F}} = \mathbb{G}_{\theta_{\mathbf{F}}}(\mathbf{F})$.

We denote that $\mathbf{F} \sim \mathcal{N}(\boldsymbol{\mu}, \mathbf{K})$. Since \mathbf{U} is sufficient for \mathbf{F} , according to the Fisher–Neyman factorization theorem,⁴ there exist non-negative functions γ and β , such that

$$p(\mathbf{F}; \boldsymbol{\mu}, \mathbf{K}) = \gamma(\mathbf{U}; \boldsymbol{\mu}, \mathbf{K})\beta(\mathbf{F}) \quad (42)$$

where γ depends on $(\boldsymbol{\mu}, \mathbf{K})$ and the sufficient statistic \mathbf{U} , while β does not depend on $(\boldsymbol{\mu}, \mathbf{K})$. Note that $\mathbf{F} = \mathbb{G}_{\theta_{\mathbf{F}}}^{-1}(\mathbb{G}_{\theta_{\mathbf{F}}}(\mathbf{F})) = \mathbb{G}_{\theta_{\mathbf{F}}}^{-1}(\tilde{\mathbf{F}})$. Let

$$p(\mathbf{F}; \boldsymbol{\mu}, \mathbf{K}) = p\left(\mathbb{G}_{\theta_{\mathbf{F}}}^{-1}(\tilde{\mathbf{F}}); \boldsymbol{\mu}, \mathbf{K}\right) \triangleq \pi(\tilde{\mathbf{F}}; \boldsymbol{\mu}, \mathbf{K}). \quad (43)$$

Moreover, since

$$p\left(\mathbb{G}_{\theta_{\mathbf{F}}}^{-1}(\tilde{\mathbf{F}}); \boldsymbol{\mu}, \mathbf{K}\right) = \gamma(\mathbf{U}; \boldsymbol{\mu}, \mathbf{K})\beta(\mathbb{G}_{\theta_{\mathbf{F}}}^{-1}(\tilde{\mathbf{F}})) \triangleq \gamma(\mathbf{U}; \boldsymbol{\mu}, \mathbf{K})\beta^*(\tilde{\mathbf{F}}), \quad (44)$$

we have

$$\pi(\tilde{\mathbf{F}}; \boldsymbol{\mu}, \mathbf{K}) = \gamma(\mathbf{U}; \boldsymbol{\mu}, \mathbf{K})\beta^*(\tilde{\mathbf{F}}), \quad (45)$$

which implies that \mathbf{U} is sufficient for $\tilde{\mathbf{F}}$ according to the Fisher–Neyman factorization theorem.

- 2) Then following the similar reasoning, we can prove that if \mathbf{U} is sufficient statistic for $\tilde{\mathbf{F}}$, then $\tilde{\mathbf{U}}$ is sufficient statistic for $\tilde{\mathbf{F}}$.
 3) Together step 1) and 2), we can conclude that if \mathbf{U} is sufficient for \mathbf{F} , then $\tilde{\mathbf{U}}$ is sufficient statistic for $\tilde{\mathbf{F}}$. \square

D. Detailed Derivations for Mean-Field ELBO

$$\begin{aligned} \text{ELBO} &= \mathbb{E}_{q(\mathbf{x}, \tilde{\mathbf{F}}, \tilde{\mathbf{U}})} \left[\log \frac{p(\tilde{\mathbf{F}}, \tilde{\mathbf{U}}, \mathbf{X}, \mathbf{Y})}{q(\mathbf{X}, \tilde{\mathbf{F}}, \tilde{\mathbf{U}})} \right] \\ &= \mathbb{E} \left[\log \frac{p(\mathbf{x}_0) \cdot p(\mathbf{U}) \mathbf{J}_{\mathbf{u}} \cdot p(\mathbf{F} | \mathbf{U}) \mathbf{J}_{\mathbf{f}} \prod_{t=1}^T p(\mathbf{y}_t | \mathbf{x}_t) p(\mathbf{x}_t | \tilde{\mathbf{f}}_t)}{q(\mathbf{x}_0) \prod_{t=1}^T q(\mathbf{x}_t | \mathbf{x}_{t-1}) q(\mathbf{U}) \mathbf{J}_{\mathbf{u}} \cdot p(\mathbf{F} | \mathbf{U}) \mathbf{J}_{\mathbf{f}}} \right] \\ &= \mathbb{E}_{q(\mathbf{x}, \tilde{\mathbf{F}}, \tilde{\mathbf{U}})} \left[\log \frac{p(\mathbf{U}) p(\mathbf{x}_0) \prod_{t=1}^T p(\mathbf{y}_t | \mathbf{x}_t) p(\mathbf{x}_t | \tilde{\mathbf{f}}_t)}{q(\mathbf{U}) q(\mathbf{x}_0) \prod_{t=1}^T q(\mathbf{x}_t | \mathbf{x}_{t-1})} \right] \\ &= \underbrace{\int_{\mathbf{x}_{0:T}} q(\mathbf{x}_{0:T}) \log \prod_{t=1}^T p(\mathbf{y}_t | \mathbf{x}_t)}_{\text{term 1}} + \underbrace{\int_{\mathbf{x}_0} q(\mathbf{x}_0) \log \frac{p(\mathbf{x}_0)}{q(\mathbf{x}_0)}}_{\text{term 2}} + \underbrace{\int_{\{\tilde{\mathbf{U}}, \tilde{\mathbf{F}}\}} q(\tilde{\mathbf{U}}) p(\tilde{\mathbf{F}} | \tilde{\mathbf{U}}) \log \frac{p(\mathbf{U})}{q(\mathbf{U})}}_{\text{term 3}} \\ &\quad + \underbrace{\int_{\mathbf{x}_{0:T}} q(\mathbf{x}_{0:T}) q(\mathbf{x}_{1:T} | \mathbf{x}_0) \log \frac{1}{q(\mathbf{x}_{1:T} | \mathbf{x}_0)}}_{\text{term 4}} + \underbrace{\int_{\{\mathbf{x}_{0:T}, \tilde{\mathbf{U}}, \tilde{\mathbf{F}}\}} q(\mathbf{x}_{0:T}) q(\tilde{\mathbf{U}}) p(\tilde{\mathbf{F}} | \tilde{\mathbf{U}}) \log \prod_{t=1}^T p(\mathbf{x}_t | \tilde{\mathbf{f}}_t)}_{\text{term 5}} \end{aligned} \quad (46)$$

Proposition 1. *The optimal $q^*(\mathbf{x}_{0:T})$ for maximizing the ELBO (cf. Eq. (46)) is Markov-structured.*

Proof. The optimal distribution for $q(\mathbf{x}_{0:T})$ is a stationary point of the ELBO. The ELBO has a stationary point w.r.t. the distribution $q(\mathbf{x}_{0:T})$ if and only if this distribution satisfies the Euler-Lagrange equation, i.e.,

$$\frac{\partial}{\partial q(\mathbf{x}_{0:T})} \left\{ q(\mathbf{x}_{0:T}) \log \prod_{t=1}^T p(\mathbf{y}_t | \mathbf{x}_t) + q(\mathbf{x}_0) \log p(\mathbf{x}_0) - q(\mathbf{x}_{0:T}) \log q(\mathbf{x}_{0:T}) + q(\mathbf{x}_{0:T}) \mathbb{E}_{q(\tilde{\mathbf{U}}) p(\tilde{\mathbf{F}} | \tilde{\mathbf{U}})} \left[\log \prod_{t=1}^T p(\mathbf{x}_t | \tilde{\mathbf{f}}_t) \right] \right\} = 0 \quad (47)$$

which implies that the optimal distribution $q^*(\mathbf{x}_{0:T})$ satisfies

$$\log \prod_{t=1}^T p(\mathbf{y}_t | \mathbf{x}_t) + \log p(\mathbf{x}_0) - \log q^*(\mathbf{x}_{0:T}) - 1 + \sum_{t=1}^T \underbrace{\mathbb{E}_{q(\mathbf{U})} [\mathbb{E}_{p(\mathbf{f}_t | \mathbf{U}, \mathbf{x}_{t-1})} [\log p(\mathbf{x}_t | \mathbb{G}_{\theta_{\mathbf{F}}}(\mathbf{f}_t))]]}_{\triangleq \Psi(\mathbf{x}_{t-1:t})} = 0, \quad (48)$$

⁴G. Casella and R. L. Berger, *Statistical inference*, 2nd ed. Cengage Learning, 2001.

where the function $\Psi(\mathbf{x}_{t-1:t})$ only depends on \mathbf{x}_{t-1} and \mathbf{x}_t after marginalizing out \mathbf{f}_t and \mathbf{U} (Generally, there is no analytical solution for integrating out \mathbf{f}_t and \mathbf{U} because of the nonlinearity of $\mathbb{G}_{\theta_F}(\cdot)$). Taking exponentiation on both sides of Eq. (48), we get the optimal distribution $q^*(\mathbf{x}_{0:T})$

$$q^*(\mathbf{x}_{0:T}) \propto p(\mathbf{x}_0) \prod_{t=1}^T p(\mathbf{y}_t | \mathbf{x}_t) \exp[\Psi(\mathbf{x}_{t-1:t})], \quad (49)$$

where $\exp[\Psi(\mathbf{x}_{t-1:t})]$ can be interpreted as an implicit transition function of the Markov SSM, and the optimal distribution of $q^*(\mathbf{x}_{0:T})$ is the corresponding smoothing distribution, which is Markov-structured. \square

Remark 6. In the GPSSM work [11], since the GP function values \mathbf{f}_t and \mathbf{U} can be analytically marginalized out, the optimal variational distribution $q^*(\mathbf{x}_{0:T})$ is a smoothing distribution of a simpler SSM and can be obtained by using particle filters. However, in the TGPSSM, the nonlinearity of $\mathbb{G}_{\theta_F}(\cdot)$ makes no closed-form solution for the integration over \mathbf{f}_t , see Eq. (48), resulting in no closed-form for the Markovian SSM in Eq. (49), thus the variational algorithm in [11] using particle filter cannot be directly applied to the TGPSSM.

Proof of Theorem 3. Next, we detail the five terms in the ELBO (cf. Eq. (46)).

- **Term 1**

$$\text{term 1} = \mathbb{E}_{q(\mathbf{x}_{0:T})} \left[\sum_{t=1}^T \log p(\mathbf{y}_t | \mathbf{x}_t) \right] = \sum_{t=1}^T \mathbb{E}_{q(\mathbf{x}_{t-1})q(\mathbf{x}_t | \mathbf{x}_{t-1})} [\log p(\mathbf{y}_t | \mathbf{x}_t)].$$

According to Eq. (26), $q(\mathbf{x}_t | \mathbf{x}_{t-1}) = \mathcal{N}(\mathbf{x}_t | \boldsymbol{\omega}_\phi(\mathbf{x}_{t-1}, \mathbf{y}_{1:T}), \boldsymbol{\Sigma}_\phi(\mathbf{x}_{t-1}, \mathbf{y}_{1:T}))$, and $p(\mathbf{y}_t | \mathbf{x}_t) = \mathcal{N}(\mathbf{y}_t | \mathbf{C}\boldsymbol{\omega}_{\mathbf{x}_t}, \mathbf{R})$ is Gaussian, thus term 1 exists closed-form solution (cf. the result in Appx. H),

$$\begin{aligned} \text{term 1} &= \sum_{t=1}^T \mathbb{E}_{q(\mathbf{x}_{t-1})} [\mathbb{E}_{q(\mathbf{x}_t | \mathbf{x}_{t-1})} [\log p(\mathbf{y}_t | \mathbf{x}_t)]] \\ &= \sum_{t=1}^T \mathbb{E}_{q(\mathbf{x}_{t-1})} \left[\log \mathcal{N}(\mathbf{y}_t | \mathbf{C}\boldsymbol{\omega}_{\mathbf{x}_t}, \mathbf{R}) - \frac{1}{2} \text{tr} [\mathbf{R}^{-1}(\mathbf{C}\boldsymbol{\Sigma}_{\mathbf{x}_t}\mathbf{C}^\top)] \right], \end{aligned} \quad (50)$$

where for notation brevity, $\boldsymbol{\omega}_{\mathbf{x}_t} \triangleq \boldsymbol{\omega}_\phi(\mathbf{x}_{t-1}, \mathbf{y}_{1:T})$ and $\boldsymbol{\Sigma}_{\mathbf{x}_t} \triangleq \boldsymbol{\Sigma}_\phi(\mathbf{x}_{t-1}, \mathbf{y}_{1:T})$. Term 1 represents the overall data fitting performance averaged over all latent states generated from their joint distribution $q(\mathbf{x}_{1:T})$, which encourages accurate reconstruction of the observations.

- **Term 2:** We assume $q(\mathbf{x}_0) = \mathcal{N}(\mathbf{x}_0 | \mathbf{m}_0, \mathbf{L}_0\mathbf{L}_0^\top)$ and $p(\mathbf{x}_0) = \mathcal{N}(\mathbf{x}_0 | \mathbf{0}, \mathbf{I})$ are both Gaussian, thus the term 2 has closed-form solution:

$$\begin{aligned} \text{term 2} &= -\mathbb{E}_{q(\mathbf{x}_0)} \log \frac{q(\mathbf{x}_0)}{p(\mathbf{x}_0)} \\ &= -\text{KL}(q(\mathbf{x}_0) \| p(\mathbf{x}_0)) \\ &= -\frac{1}{2} [(\mathbf{m}_0^\top \mathbf{m}_0) + \text{tr}(\mathbf{L}_0\mathbf{L}_0^\top) - \log |\mathbf{L}_0\mathbf{L}_0^\top| - d_x] \quad (\text{result from Appx. J}) \\ &= -\frac{1}{2} [(\mathbf{m}_0^\top \mathbf{m}_0) + \text{tr}(\mathbf{L}_0\mathbf{L}_0^\top) - 2 \log |\mathbf{L}_0| - d_x] \end{aligned} \quad (51)$$

Term 2 represents a regularization term for $q(\mathbf{x}_0)$, which encourages $q(\mathbf{x}_0)$ not staying too “far away” from $p(\mathbf{x}_0)$.

- **Term 3:**

$$\begin{aligned} \text{term 3} &= \int_{\{\tilde{\mathbf{U}}, \tilde{\mathbf{F}}\}} q(\tilde{\mathbf{U}})p(\tilde{\mathbf{F}} | \tilde{\mathbf{U}}) \log \frac{p(\mathbf{U})}{q(\mathbf{U})} d\tilde{\mathbf{F}}d\tilde{\mathbf{U}} \\ &= \int_{\tilde{\mathbf{U}}} q(\tilde{\mathbf{U}}) \log \frac{p(\mathbf{U})}{q(\mathbf{U})} d\tilde{\mathbf{U}} \quad (\text{integrate out } \tilde{\mathbf{F}}) \\ &= \int_{\mathbf{U}} q(\mathbf{U}) \log \frac{p(\mathbf{U})}{q(\mathbf{U})} d\mathbf{U} \quad (\text{LOTUS rule, see Appx. E}) \\ &= -\text{KL}[q(\mathbf{U}) \| p(\mathbf{U})] \\ &= -\frac{1}{2} \left[\mathbf{m}^\top \mathbf{K}_{\mathbf{Z}, \mathbf{Z}}^{-1} \mathbf{m} + \text{tr} \left(\mathbf{K}_{\mathbf{Z}, \mathbf{Z}}^{-1} \mathbf{S} \right) - \log \frac{|\mathbf{S}|}{|\mathbf{K}_{\mathbf{Z}, \mathbf{Z}}|} - Md_x \right] \quad (\text{result from Appx. J}) \end{aligned} \quad (52)$$

where $p(\mathbf{U}) = \mathcal{N}(\mathbf{U} | \mathbf{0}, \mathbf{K}_{\mathbf{Z}, \mathbf{Z}})$ and $q(\mathbf{U}) = \mathcal{N}(\mathbf{U} | \mathbf{m}, \mathbf{S})$. Term 3 represents a regularization term for the GP transition, which encourages $q(\mathbf{U})$ not staying too “far away” from the prior $p(\mathbf{U})$.

- **Term 4**

$$\begin{aligned}
\text{term 4} &= -\mathbb{E}_{q(\mathbf{x}_0)} \left[\mathbb{E}_{q(\mathbf{x}_{1:T}|\mathbf{x}_0)} [\log q(\mathbf{x}_{1:T}|\mathbf{x}_0)] \right] \\
&= -\mathbb{E}_{q(\mathbf{x}_0)} \left[\int_{\mathbf{x}_{1:T}} \prod_{t=1}^T q(\mathbf{x}_t|\mathbf{x}_{t-1}) \left[\sum_{t=1}^T \log q(\mathbf{x}_t|\mathbf{x}_{t-1}) \right] d\mathbf{x}_{1:T} \right] \\
&= \sum_{t=1}^T \mathbb{E}_{q(\mathbf{x}_{t-1})} \left[\underbrace{-\mathbb{E}_{q(\mathbf{x}_t|\mathbf{x}_{t-1})} [\log q(\mathbf{x}_t|\mathbf{x}_{t-1})]}_{\text{entropy}} \right] \\
&= \sum_{t=1}^T \mathbb{E}_{q(\mathbf{x}_{t-1})} \left[\frac{d_x}{2} \log(2\pi) + \frac{1}{2} \log |\Sigma_{\mathbf{x}_t}| + \frac{1}{2} d_x \right] \quad (\text{result from Theorem 4}) \tag{53}
\end{aligned}$$

Term 4 is the differential entropy term of the latent state trajectory. From Eq. (53), we can see that maximizing the ELBO essentially encourages “stretching” every \mathbf{x}_t so that the approximated smoothing distribution over the state trajectories $q(\mathbf{x}_{1:T}|\mathbf{x}_0)$ will not be overly tight.

- **Term 5**

$$\begin{aligned}
\text{term 5} &= \mathbb{E}_{q(\mathbf{x}_{0:T}, \tilde{\mathbf{U}}, \tilde{\mathbf{F}})} \left[\sum_{t=1}^T \log p(\mathbf{x}_t | \tilde{\mathbf{f}}_t) \right] \\
&= \mathbb{E}_{q(\mathbf{x}_{0:T}, \mathbf{U}, \mathbf{F})} \left[\sum_{t=1}^T \log p(\mathbf{x}_t | \mathbb{G}_{\theta_F}(\mathbf{f}_t)) \right] \quad (\text{LOTUS rule in Section E}) \\
&= \sum_{t=1}^T \mathbb{E}_{q(\mathbf{x}_{t-1:t}, \mathbf{U}, \mathbf{f}_t)} [\log p(\mathbf{x}_t | \mathbb{G}_{\theta_F}(\mathbf{f}_t))] \\
&= \sum_{t=1}^T \mathbb{E}_{q(\mathbf{x}_{t-1:t}, q(\mathbf{f}_t))} [\log p(\mathbf{x}_t | \mathbb{G}_{\theta_F}(\mathbf{f}_t))] \quad (\text{integrate out } \mathbf{U}) \tag{54} \\
&\approx \sum_{t=1}^T \mathbb{E}_{q(\mathbf{x}_{t-1:t})} \left[\frac{1}{n} \sum_{i=1}^n \log p(\mathbf{x}_t | \mathbb{G}_{\theta_F}(\mathbf{f}_t^{(i)})) \right], \quad \mathbf{f}_t^{(i)} \sim q(\mathbf{f}_t), i = 1, 2, \dots, n \tag{55}
\end{aligned}$$

where integrating out \mathbf{U} in Eq. (54) is

$$q(\mathbf{f}_t) = \int_{\mathbf{U}} q(\mathbf{f}_t, \mathbf{U}) d\mathbf{U} = \int_{\mathbf{U}} q(\mathbf{U}) p(\mathbf{f}_t | \mathbf{x}_{t-1}, \mathbf{U}) d\mathbf{U} = \mathcal{N}(\mathbf{f}_t | \mathbf{m}_{\mathbf{f}_t}, \Sigma_{\mathbf{f}_t}) \tag{56}$$

and

$$\begin{cases} \mathbf{m}_{\mathbf{f}_t} = K_{\mathbf{x}_{t-1}, \mathbf{z}} K_{\mathbf{z}, \mathbf{z}}^{-1} \mathbf{m} \\ \Sigma_{\mathbf{f}_t} = K_{\mathbf{x}_{t-1}, \mathbf{x}_{t-1}} - K_{\mathbf{x}_{t-1}, \mathbf{z}} K_{\mathbf{z}, \mathbf{z}}^{-1} [K_{\mathbf{z}, \mathbf{z}} - \mathbf{S}] K_{\mathbf{z}, \mathbf{z}}^{-1} K_{\mathbf{z}, \mathbf{x}_{t-1}} \end{cases}$$

Term 5 represents the reconstruction of the latent state trajectories, which encourages the \mathbf{f}_t sampled from GP transition $q(\mathbf{f}_t)$ to accurately reconstruct the latent state \mathbf{x}_t (from $q(\mathbf{x}_t)$). In other words, this term measures the quality of learning/fitting the underlying dynamical function.

- Therefore, the ELBO in (46) eventually becomes

$$\begin{aligned}
\text{ELBO} &\approx \sum_{t=1}^T \mathbb{E}_{q(\mathbf{x}_{t-1})} \left[\log \mathcal{N}(\mathbf{y}_t | \mathbf{C}\omega_{\mathbf{x}_t}, \mathbf{R}) - \frac{1}{2} \text{tr} [\mathbf{R}^{-1}(\mathbf{C}\Sigma_{\mathbf{x}_t} \mathbf{C}^\top)] \right] \\
&\quad - \frac{1}{2} [(\mathbf{m}_0^\top \mathbf{m}_0) + \text{tr}(\mathbf{L}_0 \mathbf{L}_0^\top) - 2 \log |\mathbf{L}_0| - d_x] \\
&\quad - \frac{1}{2} \left[\mathbf{m}^\top \mathbf{K}_{\mathbf{z}, \mathbf{z}}^{-1} \mathbf{m} + \text{tr}(\mathbf{K}_{\mathbf{z}, \mathbf{z}}^{-1} \mathbf{S}) - \log \frac{|\mathbf{S}|}{|\mathbf{K}_{\mathbf{z}, \mathbf{z}}|} - M d_x \right] \tag{57} \\
&\quad + \sum_{t=1}^T \mathbb{E}_{q(\mathbf{x}_{t-1})} \left[\frac{d_x}{2} \log(2\pi) + \frac{1}{2} \log |\Sigma_{\mathbf{x}_t}| + \frac{1}{2} d_x \right] \\
&\quad + \sum_{t=1}^T \mathbb{E}_{q(\mathbf{x}_{t-1:t})} \left[\frac{1}{n} \sum_{i=1}^n \log p(\mathbf{x}_t | \mathbb{G}_{\theta_F}(\mathbf{f}_t^{(i)})) \right].
\end{aligned}$$

□

E. LOTUS Rule [40]

The law of the unconscious statistician (LOTUS) is given by

$$\mathbb{E}_{p_{\tilde{\mathbf{x}}}}[h(\tilde{\mathbf{x}})] = \mathbb{E}_{p_{\mathbf{x}}}[h(\mathbb{G}(\mathbf{x}))]. \quad (58)$$

That is, expectations w.r.t. the transformed density $p_{\tilde{\mathbf{x}}}$ can be computed without explicitly knowing $p_{\tilde{\mathbf{x}}}$, thus saving the computation of the determinant Jacobian terms.

F. Variational Expectation

Assume $p(\mathbf{x}) = \mathcal{N}(\mathbf{x} | \boldsymbol{\mu}, V)$, $q(\mathbf{x}) \sim \mathcal{N}(\mathbf{x} | \mathbf{m}, \Sigma)$, the expectation $E_{q(\mathbf{x})}[\log p(\mathbf{x})]$ has close-form solution and is given by

$$\begin{aligned} E_{q(\mathbf{x})}[\log p(\mathbf{x})] &= E_{q(\mathbf{x})} \left[\ln \left(\frac{1}{\sqrt{(2\pi)^n |V|}} \cdot \exp \left[-\frac{1}{2}(\mathbf{x} - \boldsymbol{\mu})^T V^{-1}(\mathbf{x} - \boldsymbol{\mu}) \right] \right) \right] \\ &= -\frac{1}{2} E_{q(\mathbf{x})} [n \ln(2\pi) + \ln |V| + (\mathbf{x} - \boldsymbol{\mu})^T V^{-1}(\mathbf{x} - \boldsymbol{\mu})] \\ &= -\frac{1}{2} E_{q(\mathbf{x})} [n \ln(2\pi) + \ln |V| + \text{tr}(V^{-1} \mathbf{x} \mathbf{x}^T) - 2\boldsymbol{\mu}^T V^{-1} \mathbf{x} + \boldsymbol{\mu}^T V^{-1} \boldsymbol{\mu}] \\ &= -\frac{1}{2} [n \ln(2\pi) + \ln |V| + \text{tr}(V^{-1}(\mathbf{m} \mathbf{m}^T + \Sigma)) - 2\boldsymbol{\mu}^T V^{-1} \mathbf{m} + \boldsymbol{\mu}^T V^{-1} \boldsymbol{\mu}] \end{aligned}$$

G. Differential Entropy of Multivariate Normal Distribution

Theorem 4. Let \mathbf{x} follow a multivariate normal distribution

$$\mathbf{x} \sim \mathcal{N}(\boldsymbol{\mu}, \Sigma), \quad \mathbf{x} \in \mathbb{R}^n$$

Then, the differential entropy of \mathbf{x} in nats is

$$\mathbb{H}(\mathbf{x}) \triangleq - \int_{\mathbf{x}} p(\mathbf{x}) \ln p(\mathbf{x}) d\mathbf{x} = \frac{n}{2} \ln(2\pi) + \frac{1}{2} \ln |\Sigma| + \frac{1}{2} n$$

Proof.

$$\begin{aligned} \mathbb{H}(\mathbf{x}) &= -\mathbb{E} \left[\ln \left(\frac{1}{\sqrt{(2\pi)^n |\Sigma|}} \cdot \exp \left[-\frac{1}{2}(\mathbf{x} - \boldsymbol{\mu})^T \Sigma^{-1}(\mathbf{x} - \boldsymbol{\mu}) \right] \right) \right] \\ &= -\mathbb{E} \left[-\frac{n}{2} \ln(2\pi) - \frac{1}{2} \ln |\Sigma| - \frac{1}{2}(\mathbf{x} - \boldsymbol{\mu})^T \Sigma^{-1}(\mathbf{x} - \boldsymbol{\mu}) \right] \\ &= \frac{n}{2} \ln(2\pi) + \frac{1}{2} \ln |\Sigma| + \frac{1}{2} \mathbb{E} [(\mathbf{x} - \boldsymbol{\mu})^T \Sigma^{-1}(\mathbf{x} - \boldsymbol{\mu})] \end{aligned}$$

The last term can be evaluated as

$$\begin{aligned} \mathbb{E} [(\mathbf{x} - \boldsymbol{\mu})^T \Sigma^{-1}(\mathbf{x} - \boldsymbol{\mu})] &= \mathbb{E} [\text{tr}((\mathbf{x} - \boldsymbol{\mu})^T \Sigma^{-1}(\mathbf{x} - \boldsymbol{\mu}))] \\ &= \mathbb{E} [\text{tr}(\Sigma^{-1}(\mathbf{x} - \boldsymbol{\mu})(\mathbf{x} - \boldsymbol{\mu})^T)] \\ &= \text{tr}(\Sigma^{-1} \mathbb{E}[(\mathbf{x} - \boldsymbol{\mu})(\mathbf{x} - \boldsymbol{\mu})^T]) \\ &= \text{tr}(\Sigma^{-1} \Sigma) \\ &= \text{tr}(I_n) \\ &= n \end{aligned}$$

Therefore the differential entropy is

$$\mathbb{H}(\mathbf{x}) = \frac{n}{2} \ln(2\pi) + \frac{1}{2} \ln |\Sigma| + \frac{1}{2} n.$$

H. Expected Log-Gaussian Likelihood

Theorem 5. Let $q(\mathbf{f}) = \mathcal{N}(\mathbf{f} \mid \boldsymbol{\mu}, \Sigma)$, and the likelihood $p(\mathbf{y} \mid \mathbf{f}) = \mathcal{N}(\mathbf{y} \mid C\mathbf{f}, \mathbf{Q})$, where C is a constant matrix, then we have

$$\mathbb{E}_{q(\mathbf{f})} [\log p(\mathbf{y} \mid \mathbf{f})] = \log \mathcal{N}(\mathbf{y} \mid C\boldsymbol{\mu}, \mathbf{Q}) - \frac{1}{2} \text{tr}(\mathbf{Q}^{-1}C\Sigma C^\top)$$

Proof. Let $\mathbf{y} \in \mathbb{R}^n$, we have

$$\begin{aligned} \log p(\mathbf{y} \mid \mathbf{f}) &= \log \left[(2\pi)^{-n/2} \det(\mathbf{Q})^{-1/2} \exp \left(-\frac{(\mathbf{y} - C\mathbf{f})^\top \mathbf{Q}^{-1} (\mathbf{y} - C\mathbf{f})}{2} \right) \right] \\ &= -\frac{n}{2} \log 2\pi - \frac{1}{2} \log \det(\mathbf{Q}) - \frac{(\mathbf{y} - C\mathbf{f})^\top \mathbf{Q}^{-1} (\mathbf{y} - C\mathbf{f})}{2} \\ &= -\frac{\text{tr}(C^\top \mathbf{Q}^{-1} C \mathbf{f} \mathbf{f}^\top) - 2\mathbf{y}^\top \mathbf{Q}^{-1} C \mathbf{f} + \mathbf{y}^\top \mathbf{Q}^{-1} \mathbf{y}}{2} - \frac{n}{2} \log 2\pi - \frac{1}{2} \log \det(\mathbf{Q}) \end{aligned}$$

Therefore, we have the expected value

$$\begin{aligned} \mathbb{E}_{q(\mathbf{f})} [\log p(\mathbf{y} \mid \mathbf{f})] &= -\frac{\text{tr}(C^\top \mathbf{Q}^{-1} C \mathbb{E}_{q(\mathbf{f})} [\mathbf{f} \mathbf{f}^\top]) - 2\mathbf{y}^\top \mathbf{Q}^{-1} C \boldsymbol{\mu} + \mathbf{y}^\top \mathbf{Q}^{-1} \mathbf{y}}{2} - \frac{n}{2} \log 2\pi - \frac{1}{2} \log \det(\mathbf{Q}) \\ &= -\frac{\text{tr}[C^\top \mathbf{Q}^{-1} C (\boldsymbol{\mu} \boldsymbol{\mu}^\top + \Sigma)] - 2\mathbf{y}^\top \mathbf{Q}^{-1} C \boldsymbol{\mu} + \mathbf{y}^\top \mathbf{Q}^{-1} \mathbf{y}}{2} - \frac{n}{2} \log 2\pi - \frac{1}{2} \log \det(\mathbf{Q}) \\ &= -\frac{(\mathbf{y} - C\boldsymbol{\mu})^\top \mathbf{Q}^{-1} (\mathbf{y} - C\boldsymbol{\mu})}{2} - \frac{n}{2} \log 2\pi - \frac{1}{2} \log \det(\mathbf{Q}) - \frac{1}{2} \text{tr}(\mathbf{Q}^{-1} C \Sigma C^\top) \\ &= \log \mathcal{N}(\mathbf{y} \mid C\boldsymbol{\mu}, \mathbf{Q}) - \frac{1}{2} \text{tr}(\mathbf{Q}^{-1} C \Sigma C^\top) \end{aligned}$$

□

I. Marginal Variational Distribution $q(\mathbf{f})$ in Variational Sparse GP [42]

Suppose the variational distributions

$$q(\mathbf{f}, \mathbf{u}) = q(\mathbf{u}) p(\mathbf{f} \mid \mathbf{u}), \quad q(\mathbf{u}) = \mathcal{N}(\mathbf{u} \mid \boldsymbol{\mu}, \Sigma)$$

and

$$p(\mathbf{f} \mid \mathbf{u}) = \mathcal{N}(\mathbf{f} \mid \mathbf{m}_f + \mathbf{K}_{fu} \mathbf{K}_{uu}^{-1} (\mathbf{u} - \mathbf{m}_u), \mathbf{K}_{ff} - \mathbf{K}_{fu} \mathbf{K}_{uu}^{-1} \mathbf{K}_{fu}^\top).$$

Using Lemma 1, we have

$$\begin{aligned} q(\mathbf{f}) &= \int_{\mathbf{u}} q(\mathbf{u}) p(\mathbf{f} \mid \mathbf{u}) d\mathbf{u} \\ &= \mathcal{N}(\mathbf{f} \mid \mathbf{m}_f + \mathbf{K}_{fu} \mathbf{K}_{uu}^{-1} (\boldsymbol{\mu} - \mathbf{m}_u), \mathbf{K}_{fu} \mathbf{K}_{uu}^{-1} \Sigma \mathbf{K}_{uu}^{-1} \mathbf{K}_{fu}^\top + \mathbf{K}_{ff} - \mathbf{K}_{fu} \mathbf{K}_{uu}^{-1} \mathbf{K}_{fu}^\top) \\ &= \mathcal{N}(\mathbf{f} \mid \mathbf{m}_f + \mathbf{K}_{fu} \mathbf{K}_{uu}^{-1} (\boldsymbol{\mu} - \mathbf{m}_u), \mathbf{K}_{ff} - \mathbf{K}_{fu} \mathbf{K}_{uu}^{-1} (\mathbf{K}_{uu} - \Sigma) \mathbf{K}_{uu}^{-1} \mathbf{K}_{fu}^\top) \end{aligned}$$

Lemma 1. (Joint distribution of Gaussian variables [1]) If random variables $\mathbf{x} \in \mathbb{R}^n$ and $\mathbf{y} \mid \mathbf{x} \in \mathbb{R}^m$ have the Gaussian distributions

$$\begin{aligned} \mathbf{x} &\sim \mathcal{N}(\mathbf{m}, \mathbf{P}), \\ \mathbf{y} \mid \mathbf{x} &\sim \mathcal{N}(\mathbf{H}\mathbf{x} + \mathbf{u}, \mathbf{R}), \end{aligned}$$

then the joint distribution of \mathbf{x}, \mathbf{y} and the marginal distribution of \mathbf{y} are given as

$$\begin{aligned} \begin{pmatrix} \mathbf{x} \\ \mathbf{y} \end{pmatrix} &\sim \mathcal{N} \left(\begin{pmatrix} \mathbf{m} \\ \mathbf{H}\mathbf{m} + \mathbf{u} \end{pmatrix}, \begin{pmatrix} \mathbf{P} & \mathbf{P}\mathbf{H}^\top \\ \mathbf{H}\mathbf{P} & \mathbf{H}\mathbf{P}\mathbf{H}^\top + \mathbf{R} \end{pmatrix} \right), \\ \mathbf{y} &\sim \mathcal{N}(\mathbf{H}\mathbf{m} + \mathbf{u}, \mathbf{H}\mathbf{P}\mathbf{H}^\top + \mathbf{R}). \end{aligned}$$

J. KL Divergence Between Two Multivariate Gaussian Distributions

For the two Gaussian distributions $P = \mathcal{N}(\mathbf{x} \mid \boldsymbol{\mu}_1, \Sigma_1)$ and $Q = \mathcal{N}(\mathbf{x} \mid \boldsymbol{\mu}_2, \Sigma_2)$, their KL divergence is given by

$$\begin{aligned} \text{KL}(P \parallel Q) &= \int P(\mathbf{x}) \log \frac{P(\mathbf{x})}{Q(\mathbf{x})} d\mathbf{x} \\ &= \frac{1}{2} \left[(\boldsymbol{\mu}_2 - \boldsymbol{\mu}_1)^\top \Sigma_2^{-1} (\boldsymbol{\mu}_2 - \boldsymbol{\mu}_1) + \text{tr}(\Sigma_2^{-1} \Sigma_1) - \ln \frac{|\Sigma_1|}{|\Sigma_2|} - n \right]. \end{aligned}$$

Proof can be referred to, e.g., https://stanford.edu/~jduchi/projects/general_notes.pdf

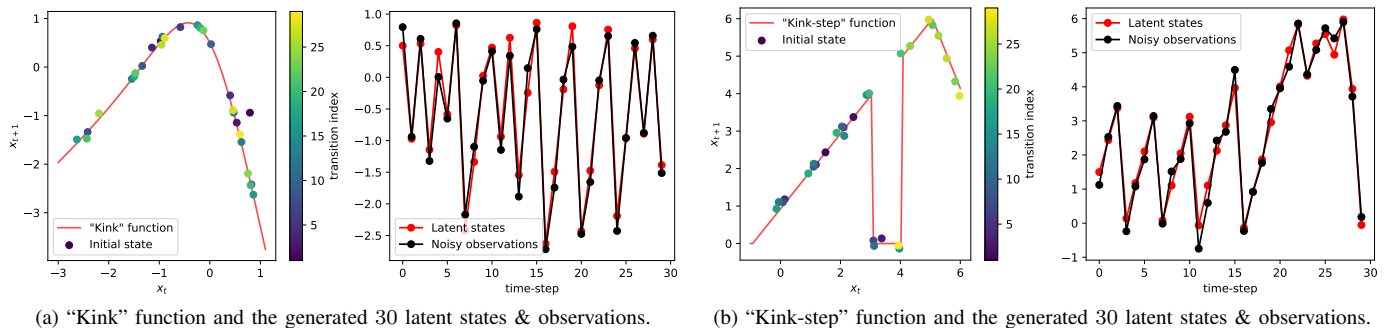


Fig. 8: The 1-D datasets (kink function and kink-step function), including the latent state trajectories and the corresponding observations.

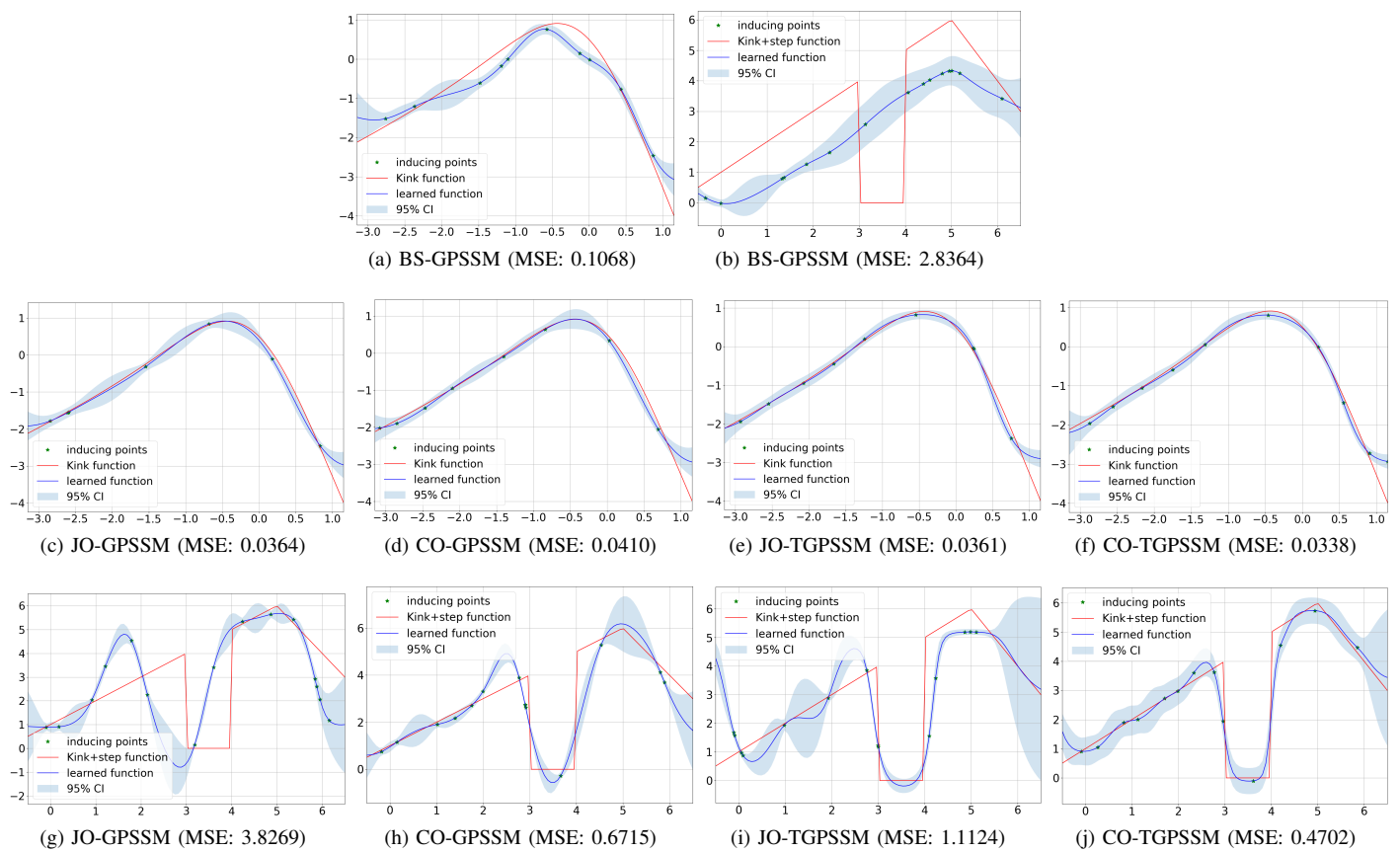


Fig. 9: Learning the “kink” and “kink-step” dynamical systems using GPSSMs and TGPSSMs.

TABLE V: Details of the system identification datasets

Dataset	Control Input	Observations	Length
Actuator	$c_t \in \mathbb{R}$	$y_t \in \mathbb{R}$	$T = 1024$
Ballbeam	$c_t \in \mathbb{R}$	$y_t \in \mathbb{R}$	$T = 1000$
Drive	$c_t \in \mathbb{R}$	$y_t \in \mathbb{R}$	$T = 500$
Dryer	$c_t \in \mathbb{R}$	$y_t \in \mathbb{R}$	$T = 1000$
Gas Furnace	$c_t \in \mathbb{R}$	$y_t \in \mathbb{R}$	$T = 296$

K. More Experimental Results

1) 1-D Datasets:

2) System Identification Datasets:

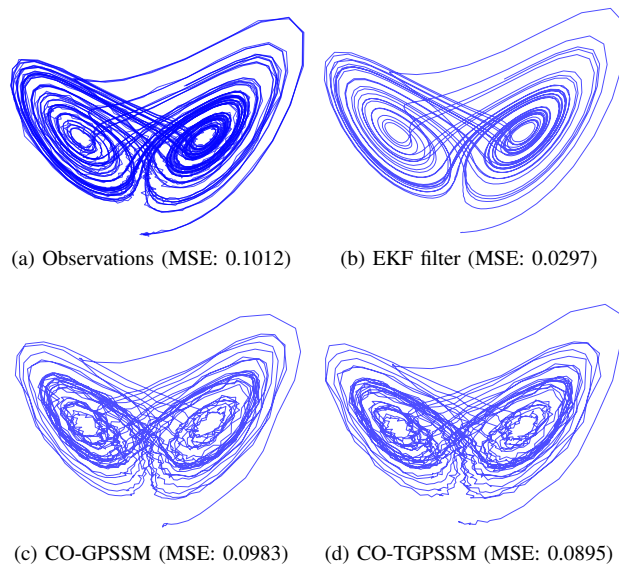


Fig. 10: Comparisons of the inferred state trajectory ($T = 2000$)